ADSORPTION OF CARBON DIOXIDE ON ZEOLITES SYNTHESIZED USING SILICA GEL WASTE

CHALIDA UPAN

A Thesis Submitted in Partial Fulfillment of the Requirements for the
Degree of Master of Science in Chemistry
Suranaree University of Technology
Academic Year 2024

การดูดซับก๊าซคาร์บอนไดออกไซด์บนซีโอไลต์ที่สังเคราะห์จากซิลิกาเจลเหลือทิ้ง

นางสาวชลิดา อุปัญญ์

วิทยานิพนธ์นี้เป็นส่วนหนึ่งของการศึกษาตามหลักสูตรปริญญาวิทยาศาสตรมหาบัณฑิต
สาขาวิชาเคมี
มหาวิทยาลัยเทคโนโลยีสุรนารี
ปีการศึกษา 2567

ADSORPTION OF CARBON DIOXIDE ON ZEOLITES SYNTHESIZED USING SILICA GEL WASTE

Suranaree University of Technology has approved this thesis submitted in partial fulfillment of the requirements for a Master's degree.

Thesis Examining Committee

(Assoc. Prof. Dr. Sanchai Prayoonpokarach)
Chairperson

(Prof. Dr. Jatuporn Wittayakun)
Member (Thesis Advisor)

(Assoc. Prof. Dr. Kamonwad Ngamchuea)
Member

(Asst. Prof. Dr. Sirinuch Loiha)
Member

(Assoc. Prof. Dr. Yupaporn Raksakulpiwat)
Vice Rector for Academic Affairs
and Quality Assurance

(Prof. Dr. Santi Maensiri)
Dean of Institute of Science

ชลิดา อุปัญญ์ : การดูดซับก๊าซคาร์บอนไดออกไซด์บนซีโอไลต์ที่สังเคราะห์จากซิลิกาเจลเหลือทิ้ง (ADSORPTION OF CARBON DIOXIDE ON ZEOLITES SYNTHESIZED USING SILICA GEL WASTE) อาจารย์ที่ปรึกษา : ศาสตราจารย์ ดร.จตุพร วิทยาคุณ, 73 หน้า.

คำสำคัญ : ซีโอไลต์ ซิลิกาเจล คาร์บอนไดออกไซด์ CO_2

การสะสมของเสียที่อยู่ในรูปของแข็งจากอุตสาหกรรมหรือการเกษตรนำไปสู่ความกังวลทางด้านสิ่งแวดล้อมเพิ่มขึ้น ของเสียบางส่วนถูกนำไปรีไซเคิลหรือแปรรูปเป็นผลิตภัณฑ์ที่มีมูลค่าเพิ่ม ความน่าสนใจของงานวิจัยนี้คือซิลิกาเจล ซึ่งใช้เป็นสารดูดความชื้นในบรรจุภัณฑ์และถูกทิ้งเป็นของเสีย โดยซิลิกาเจลมีปริมาณซิลิกาสูงซึ่งสามารถใช้เป็นสารตั้งต้นในการสังเคราะห์ซีโอไลต์ได้ งานวิจัยนี้มีวัตถุประสงค์เพื่อใช้ซิลิกาเจลเป็นแหล่งซิลิกาในการสังเคราะห์ซีโอไลต์ชนิดเอ เอ็กซ์ และ วาย จากผลการศึกษาพบว่า สามารถสังเคราะห์ซีโอไลต์ชนิดโซเดียมเอ เอ็กซ์ และวายที่บริสุทธิ์ได้ ซีโอไลต์ที่สังเคราะห์ได้จากของเสียซิลิกาเจลจะนำไปใช้เป็นตัวดูดซับในการดูดซับก๊าซคาร์บอนไดออกไซด์ ความสามารถในการดูดซับก๊าซคาร์บอนไดออกไซด์ของซีโอไลต์โซเดียมเอ, เอ็กซ์ และวาย คือ 4.10, 5.84 และ 4.39 มิลลิโมลต่อกรัม ตามลำดับ ซีโอไลต์ที่สังเคราะห์จากของเสียซิลิกาเจลมีความสามารถในการดูดซับก๊าซคาร์บอนไดออกไซด์ใกล้เคียงกับซีโอไลต์ทางการค้า จากผลการศึกษาที่ได้แสดงให้เห็นว่า ซีโอไลต์ที่สังเคราะห์จากของเสียซิลิกาเจลเป็นวัสดุดูดซับที่มีประสิทธิภาพสูง มีต้นทุนที่ต่ำ และเป็นตัวดูดซับที่เป็นมิตรกับสิ่งแวดล้อม

สาขาวิชาเคมี ลายมือชื่อนักศึกษา ชลิดา

ปีการศึกษา 2567 ลายมือชื่ออาจารย์ที่ปรึกษา จตุพร วิทยาคุณ

CHALIDA UPAN : ADSORPTION OF CARBON DIOXIDE ON ZEOLITES SYNTHESIZED USING SILICA GEL WASTE. THESIS ADVISOR : PROF. JATUPORN WITTAYAKUN, Ph.D. 73 PP.

Keyword: zeolites silica gel carbon dioxide CO_2

Accumulation of industrial or agricultural solid waste leads to increased environmental concern. Some solid waste should be recycled or converted to value-added products. The interest of this research is silica gel, commonly used as a desiccant in packaging and discarded as solid waste. Silica gel has a high percentage of silica which can be used as a precursor in zeolite synthesis. This work aims to use silica gel waste as a silica source to synthesize zeolite A, X and Y. The results showed phase-pure of zeolites A, X, and Y in sodium forms. The synthesized zeolites obtained from silica gel waste are used as adsorbents for the CO_2 adsorption. The CO_2 adsorption capacities of NaA, NaX and NaY were 4.10, 5.84 and 4.39 mmol/g, respectively. The synthesized zeolite samples generally show adsorption capacity values similar to those of the commercial zeolites. The study demonstrates that zeolites produced from silica gel waste are highly efficient adsorbents with low costs and environmentally friendly absorbents.

School of Chemistry
Academic Year 2024

Student's Signature ชลิดา
Advisor's Signature จตุพร วิทยากุล

ACKNOWLEDGEMENTS

I am deeply grateful to Prof. Dr. Jatuporn Wittayakun for his invaluable guidance, constructive feedback, unwavering support, and for continually inspiring me with fascinating research projects. This work would not have been possible without his encouragement, insight, and collaboration.

I sincerely appreciate my mentor, Dr. Chalermpan Keawkumay, for his dedication in the laboratory, thoughtful feedback, continuous encouragement, and invaluable guidance throughout my research journey.

I would also like to extend my gratitude to all JW group members for their constant support and encouragement. I feel truly fortunate to be part of such an inspiring and collaborative team.

Special thanks to Saran Youngjan, Pawan Boonyoung, and Dr. Pongtanawat Khemthong from the National Nanotechnology Center (NANOTEC), National Science and Technology Development Agency (NSTDA), Thailand, for their generous assistance with CO_2 adsorption studies.

Most importantly, I am profoundly grateful to my family for their unconditional love and unwavering support in every aspect of my life. Their belief in me has been my greatest motivation.

Chalida Upan

CONTENTS

CONTENTS (Continued)

LIST OF TABLES

LIST OF FIGURES

LIST OF FIGURES (Continued)

LIST OF ABBREVIATION

RHA	Rice husk Ash
Ref.	Reference
LTA	Linde Type A
FAU	Faujasite-type
CCUS	Carbon Capture, Utilization, and Storage
ZSM-5	Zeolite Socony Mobil
SCBA	Sugarcane Bagasse Ash
h	Hour
nm	Nanometer
D6Rs	Double Six-Membered Ring
MRs	Membered Ring
EDXRF	Energy Dispersive X-ray Fluorescence
min	Minute
g	Gram
XRD	X-ray diffraction
SEM-EDX	Scanning electron microscopy with energy dispersive X-ray spectroscopy
FTIR-ATR	Attenuated Total Reflection Fourier Transform Infrared Spectroscopy
BET	Brunauer-Emmett-Teller
TPD	Temperature-Programmed Desorption
kPa	Kilopascal
μm	Micrometer
mg	Milligram
EO	Essential oils
MOFs	Metal-Organic Frameworks
MOR	Mordenite
CD	Cyclodextrins

LIST OF ABBREVIATIONS (Continued)

RPMs	Recyclable Porous Material
EB	Ethyl butyrate
FG	Fragrance
DL	D-limonene
EEO	Eucalyptus Essential Oil
EO	Essential oil
MS	Methyl salicylate
RH	Rice husk
TGA	Thermogravimetric Analysis
rpm	Revolutions Per Minute
pH	Potential of Hydrogen
PP	Polypropylene
mL	Millileter
GC-FID	Gas Chromatography-Flame Ionization Detection
ppm	Parts Per Million
µL	Microliter

CHAPTER I
INTRODUCTION

1.1 Introduction

The combustion of fossil fuels generates substantial CO_2 emissions, making it the largest source of anthropogenic greenhouse gases. Therefore, post-combustion CO_2 capture, along with its proper utilization or disposal, is essential in power plants to enhance the sustainability of energy production from fossil fuels, such as coal (de Aquino et al., 2020; Muriithi et al., 2020).

There are several techniques for CO_2 removal. The development of CO_2 capture through adsorption on solid sorbents has gained significant interest due to its low energy requirements, simplicity, and cost-effectiveness (Kaithwas et al., 2012; Keawkumay et al., 2024).

Zeolites are commonly used in a range of applications, including ion exchange for water purification, catalysis, detergent formulation, building materials, and gas adsorption, especially CO_2. Zeolites are especially recognized as adsorbents. Their high adsorption capacity is attributed to their excellent thermal stability, stable crystalline structure, low density, uniformly sized channels, large surface area, and substantial pore volume (de Carvalho Izidoro et al., 2024). Zeolites are crystalline microporous aluminosilicates consisting of tetrahedral TO_4 units (T = Si or Al) interconnected through shared oxygen atoms (Wittayakun et al., 2008). The silicon-to-aluminum ratio (Si/Al) significantly affects the zeolite structure and adsorption capacity.

One of the challenges in zeolite synthesis is the high energy consumption and the use of silica sources which are non-environmentally friendly, for example, fumed silica and silicon alkoxides (Sharma et al., 2015). Recently, there has been increasing interest in synthesizing zeolites from low-cost materials, including rice husk, fly ash, rice husk ash, and kaolin. Additionally, silica derived from waste materials, such as

silica gel waste, has proven to be a promising raw material for the synthesis of zeolites due to its high silica content (Khaosomboon et al., 2018).

Silica gel is commonly used as a desiccant, adsorbent, or in chromatography, but improper disposal can lead to environmental challenges. The continuous increase in silica gel waste has made its disposal a growing concern. Converting this waste into value-added products offers a sustainable solution. Due to its high silica (silicon dioxide) content, silica gel waste can serve as a valuable precursor for zeolite synthesis.

This research aims to synthesize zeolites NaA, NaX, and NaY using a silica source from silica gel waste and to compare their CO_2 adsorption capacity to commercial zeolites. The study also examines the effect of the Si/Al ratio on adsorption performance. Additionally, the physicochemical properties, morphology, basicity and N_2 adsorption–desorption isotherms of the synthesized zeolites derived from silica gel waste are analyzed and discussed.

In addition to the main thesis body, an unsuccessful study of the adsorption of wintergreen and eucalyptus essential oils onto synthesized zeolites from fumed silica is reported in the Appendix. The issue was attributed to the zeolite's low adsorption capacity for fragrance molecules, which hindered the precise determination of the adsorbate amount. The research details, including methodology and data, can be found in the Appendix.

1.2 Objectives

This study aims to achieve three key objectives. First, it emphasizes the synthesis of phase-pure zeolites NaA, NaX, and NaY from silica gel waste as a silica source using the hydrothermal method. Second, it aims to evaluate the CO_2 adsorption capacity of the synthesized zeolites (NaA, NaX, and NaY) in comparison with their commercial counterparts to assess their performance. Lastly, the study aims to examine the effect of the zeolite Si/Al ratio and framework structure on adsorption capacity, providing insights into how these factors affect CO_2 capture efficiency.

CHAPTER II
LITERATURE REVIEWS

2.1 Zeolite

Zeolites are crystalline microporous aluminosilicates with three-dimensional structures composed of $[SiO_4]^{4-}$ and $[AlO_4]^{5-}$ tetrahedra linked by sharing oxygen atoms. There are several structural types with various cavity sizes, typically 0.3 to 1.0 nm, formed by linking pore openings of specific sizes within the tetrahedral framework. The presence of $[AlO_4]^{5-}$ tetrahedra results in the framework's negative charge, which requires a charge-balancing cation. The general formula of zeolite is $M_{a/n}[(AlO_2)_a(SiO_2)_b]\cdot cH_2O$, where M represents charge-balancing cation of alkali or alkaline earth metal, *n* denotes the valence of the metal cation, *c* indicates the number of water molecules per unit cell, and *a* and *b* represent the total number of $[SiO_4]^{4-}$ and $[AlO_4]^{5-}$ tetrahedra in the zeolite's unit cell, respectively (Lakiss et al., 2020). The ratio *b/a* varies from 1.0 to 5.0 but can be adjusted depending on the zeolite's structure.

Zeolites are generally classified into two main categories: natural and synthetic zeolites. While natural zeolites are abundant, more emphasis is now placed on synthesizing zeolites because they can be produced in pure form, offer improved ion exchange capabilities, and have uniform particle sizes. They are also utilized as adsorbents, catalysts or molecular sieves, removal of heavy metals, gas capture, and various other applications (Khaleque et al., 2020) due to their porosity and ion-exchange capabilities (Yilmaz and Müller, 2009). Recently, significant attention has been focused on synthesizing zeolites from low-cost materials (Table 1). Rice husk, rice husk ash, fly ash, paper sludge, kaolin, and other silica- and alumina-rich materials can serve as raw materials for zeolite synthesis.

Table 1 The benefits and limitations of various raw materials in synthetic zeolite production (Abdullahi et al., 2017).

Raw materials	Chemical composition (%)	Advantages	Disadvantages	Zeolite	Ref.
RHA	80% SiO_2, Al_2O_3, Fe_2O_3, CaO, MgO, Na_2O and K_2O, and others	Low cost, ultrafine size, highly porous and chemically reactive.	Pre-treatment of RHA and waste glasses increase the cost.	ZSM5, T, NaY	C. Zhang et al. (2019) Kamseu et al. (2017)
Clay materials (kaolin, smectite)	SiO_2 46.5, Al_2O_3 41.18, Fe_2O_3 0.19, TiO_2 0.13, MgO 0.04, K_2O 0.13, Na_2O 0.18, ZrO_2 0.01, SO_3 0.15, P_2O_5 0.03, LOI 16.25	Availability, convenient source for producing low silica zeolites like Y, use of kaolin waste for zeolite synthesis reduces the cost of reagents.	High energy consumption processes like grinding, calcination, fusion required. Raw materials mining destroys the natural landscape.	NaA, mordenite, faujasites, and, NaP	Tavasoli et al. (2014)

Table 1 (Continued) show benefits and limitations of various raw materials in synthetic zeolite production (Abdullahi et al., 2017).

Raw materials	Chemical composition (%)	Advantages	Disadvantages	Zeolite	Ref.
Coal fly ash	SiO_2 38.3, Al_2O_3 34.8, CaO 11.0, Fe_2O_3 8.1, Others 7.8	The primary Main constituents are silica and alumina, which offer the potential of converting it to zeolite, Produce low price zeolite with high purity, no harmful effect.	Effect of the impeller type and agitation during the hydrothermal treatment stage of the process.	X, Na-P1, A, Y	Amoni et al. (2019)
Silica gel waste	SiO_2 99.71	High composition of silica, uniform porous structure.	Limited alumina content	A and Y	Khaosomboon et al. (2018)

Several silica sources in zeolite synthesis include silica derived from waste materials such as rice husk and coal fly ash. A particularly promising waste source for

silica is silica gel waste, which contains a high silica content, 99.71% (Khaosomboon et al., 2018). This work presents the synthesis of zeolites LTA (NaA) and FAU (NaX and NaY) using silica gel waste as a silicon precursor.

Linde Type A (LTA) zeolite, commonly known as zeolite A, has a Si/Al ratio ranging from 1.0 to 1.5. Faujasite (FAU) zeolites exist in two forms based on their Si/Al ratio: zeolite X, with a ratio of 1.0 to 1.5, and zeolite NaY, which has a Si/Al ratio greater than 1.5. The pore diameter of LTA is 4 Å, while FAU has a larger pore diameter of 7.4 Å. Both zeolite types possess high surface areas, enhancing their adsorption capacity.

Among the various classes of zeolites, LTA and FAU are the most well-known for CO_2 capture due to their structural characteristics and Si/Al molar ratios. Figure 1 illustrates the structural units of LTA and FAU zeolites.

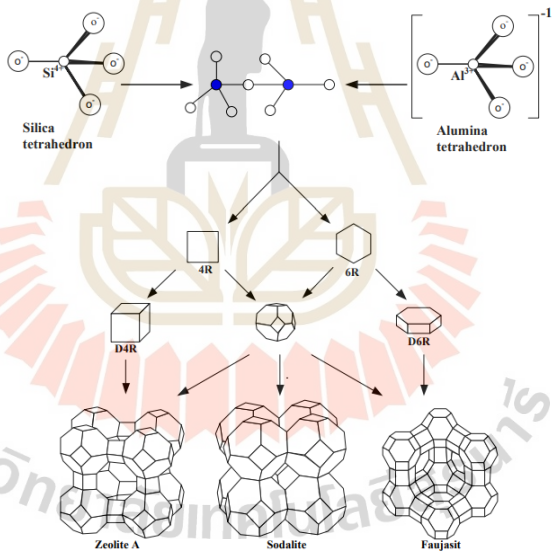

Figure 1 Structure of the LTA and FAU Zeolite Units (Masoudian et al., 2013).

2.2 Adsorption CO_2 in zeolites

The applications of zeolites are largely due to their unique properties. While zeolites are used in various fields, this research specifically focused on the use of synthesized zeolites for CO_2 adsorption.

Zeolites possess tunable channels within a rigid framework, granting them outstanding shape selectivity and efficient interaction capabilities with carbon dioxide (CO_2) molecules, the primary greenhouse gas. Large-scale CO_2 capture and utilization

are achieved through Carbon Capture, Utilization, and Storage (CCUS) technology. CO_2 capture is the process of separating and concentrating CO_2 from various emission sources using techniques like absorption, adsorption and membrane separation.

The fundamental principle of zeolite adsorption is that molecules, such as CO_2, with diameters smaller than the pore size of the zeolite, can enter and be adsorbed within the crystal. Table 2 shows a comparison of the adsorption capacity of CO_2 in zeolites.

Table 2 Comparison of CO_2 adsorption capacities in various zeolite types (Davarpanah et al., 2020).

Sample	Condition pretreatment (K)	CO_2 adsorption capacity (mmol g^{-1})	Ref.
13X	593	4.6	Khraisheh et al. (2020)
ZSM-5	573	1.6	Li et al. (2013)
	373	0.9	Wang et al. (2017)
4A	523	1.65	Siriwardane et al. (2001)
NaY and KY	393	4.4-5.18	Walton et al. (2006)
NaA from sugarcane bagasse (SCBA)	300 °C, 3 h under vacuum	1.56	Keawkumay et al. (2024)
NaA-P from SCBA	300 °C, 3 h under vacuum	4.30	Keawkumay et al. (2024)
NaA-PS from SCBA	300 °C, 3 h under vacuum	4.10	Keawkumay et al. (2024)
Commercial NaA	300 °C, 3 h under vacuum	4.38	Keawkumay et al. (2024)
Y	No treatment	2.18	Gouveia et al. (2020)

Table 2 (Continued) Comparison of CO_2 adsorption capacities in various zeolite types (Davarpanah et al., 2020).

Sample	Condition pretreatment (K)	CO_2 adsorption capacity (mmol g^{-1})	Ref.
4A	200 °C, 12 h under vacuum	3.39	Panda et al. (2019)
5A	150 °C, 12 h under vacuum	3.68	Gao et al. (2015)

Zeolite has shown strong potential as an adsorbent for CO_2 capture, with pretreatment playing a key role in enhancing adsorption performance. Specifically, the pretreatment temperature of the zeolite significantly influences its CO_2 adsorption capacity, which increases as the temperature rises (Kuceba and Nowak, 2005). This suggests that the activation temperature is an important factor in the CO_2 sorption process; the higher temperatures promote dehydration and generate additional adsorption sites (Keawkumay et al., 2024).

2.3 Mechanisms of CO_2 adsorption in zeolites

The adsorption behavior of FAU, classified as large-pore zeolites (diameter 0.60–0.80 nm), is primarily determined by electrostatic interactions. However, LTAs, classified as small-pore zeolites (diameter 0.30–0.45 nm), exhibit diffusion and size exclusion, which additionally affect adsorption behavior.

CO_2 adsorption via electrostatic interactions with the adsorbent is referred to as equilibrium separation. This interaction is influenced by factors such as the polarity and polarizability of gas molecules, as well as the electric field gradient of the zeolite surface, which becomes stronger with increased aluminum content. Despite being a nonpolar molecule, CO_2 exhibits strong adsorption on zeolites due to its significant quadrupole moment and high polarizability.

2.3.1 Mechanisms of CO_2 adsorption in zeolite FAU and LTA

The primary adsorption mechanisms proposed for medium- and large-pore zeolites are shown in Figure 2. A CO_2 oxygen atom could interact with an extra-

framework cation within the zeolite cavities (Figure 2A). Both CO_2 oxygen atoms could also bridge separate extra-framework cations (Figure 2D). Moreover, CO_2 could form carbonate species by adsorption on framework oxygen via carbon atom with interaction between CO_2 oxygen and potassium cation (Figures 2B and 2C).

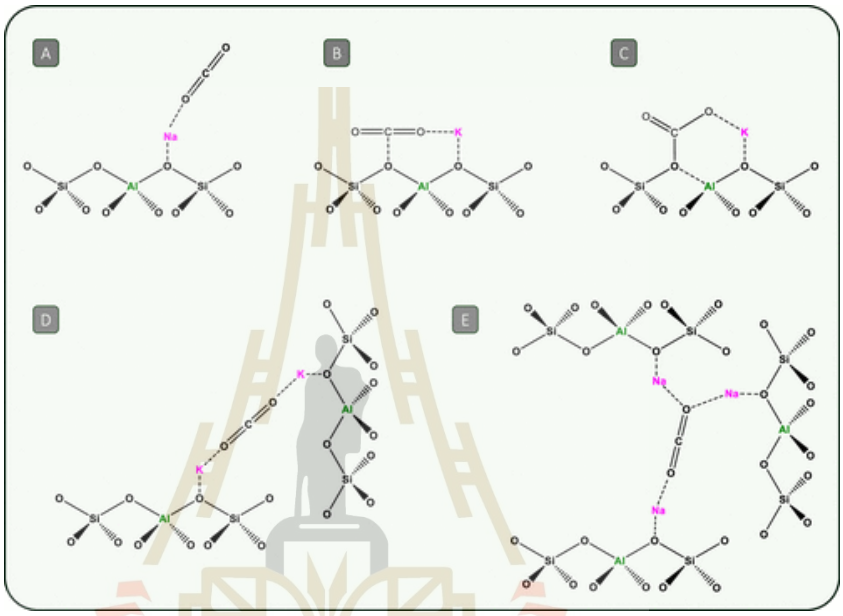

Figure 2 Mechanisms of CO_2 Interaction with zeolites (Boer et al., 2023).

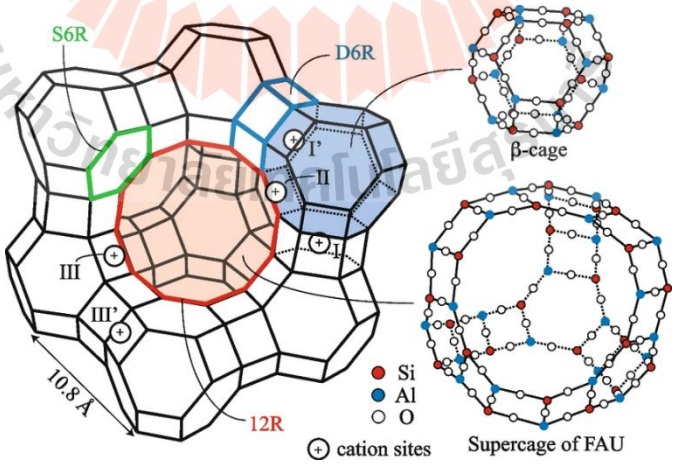

Figure 3 Schematic representation of the FAU-type framework structure (Nakano and Harashima, 2024).

Figure 3 shows the framework of FAU zeolites containing sodalite building blocks linked by double six-membered rings (D6Rs), resulting in the formation of a

supercage with a 12-membered ring (12MR) window. The sodalite cage is composed of 8 six-membered rings (6MRs) and 6 four-membered rings (4MRs). From the different Si/Al ratios, zeolite Y contains a lower amount of Al, leading to a reduced presence of extra-framework cations per mass of material. Figure 4 exhibits the positions of cations in the FAU structure (Rouquerol, 1999).

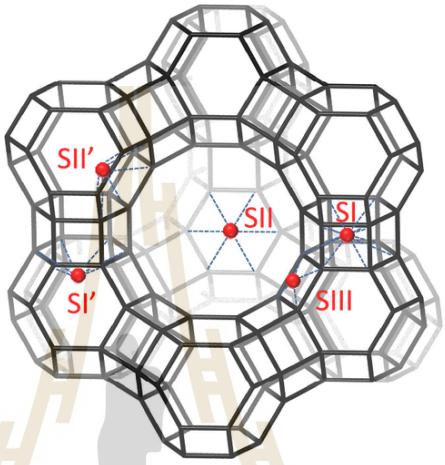

Figure 4 The potential locations of counter cations within the Faujasite structure (Norby et al., 1998).

In the FAU structure, CO_2 cannot access the cations at sites I, I′, and II′ within the D6R or sodalite cage (Figure 4). In NaX, CO_2 adsorption occurs at two sites, II and III′, within the supercage. At low CO_2 loading, CO_2 favorably interacts with site III′ cations, which is positioned slightly off from site III (site III′ is not shown in Figure 4). This may be due to the greater accessibility of these sites, as they are closer to the supercage center than site II. At higher CO_2 loading, when the type III′ sites are occupied, CO_2 additionally interacts with the cations at site II (Maurin et al., 2005). In zeolites NaY and LiY, CO_2 interacts with cations at site II because the sites III′ are unoccupied.

2.3.2 Mechanisms of CO_2 adsorption in small-pore zeolites

In small-pore zeolite A, the mechanisms are the same as medium- and large-pore zeolites. However, the accessibility of these pores becomes an important additional factor in influencing both adsorption capacity and selectivity because the pore sizes are comparable to the size of the adsorbent.

Figure 5 shows the structure of zeolite A, which is a small-pore zeolite composed of sodalite cages connected by double 4 rings (D4Rs), forming a supercage (also referred to as the **α**-cage, as shown in Figure 5) that can be accessed through 8-membered rings (8MRs). Figure 6 illustrates three cation sites in zeolite A. Cation site II is found within the window of the 8-membered ring (8MR) that allows access to the supercage. In NaA, the cation is positioned away from the center of the window, which does not significantly hinder the diffusion of CO_2 into the supercage (Boer et al., 2023).

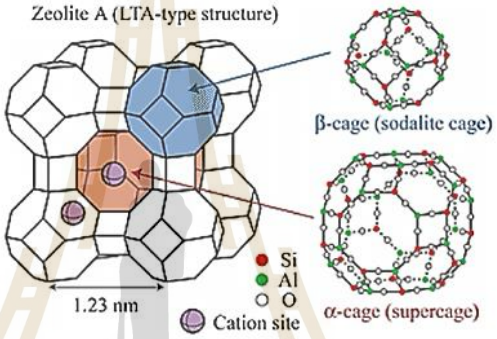

Figure 5 Schematic representation of the LTA-type framework structure (Abdullahi et al., 2017).

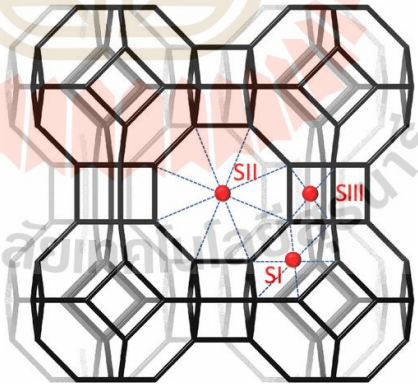

Figure 6 Cation sites for CO_2 in the LTA zeolite (Zukal et al., 2011).

2.4 Factors influencing CO_2 adsorption in zeolites

2.4.1 Type of Framework

Zeolite classifications are based on the distinct size and geometry of their channels and cages. The framework structure plays a crucial role in defining key material properties, including the number of T atoms (T = Si or Al) within the rings

and the corresponding pore size (Å). For effective CO_2 diffusion, the pore aperture must be at least 3.3 Å, meaning the framework should consist of an 8-membered ring (8MR) or larger, as smaller rings have apertures that are too restrictive. Additionally, pore size can be adjusted by incorporating alkali or alkaline earth metals, which in turn can influence the adsorption mechanism (Boer et al., 2023).

The pore structure, along with the size and geometry of a zeolite, plays a crucial role in governing adsorbate diffusion and ultimately affects its effectiveness as an adsorbent.

2.4.2 Si/Al Ratio

The Si/Al ratio in zeolites plays a crucial role in determining their adsorption capacity and selectivity for polar and polarizable molecules. Zeolites with lower Si/Al ratios have higher aluminum content, resulting in an increased number of extra-framework cations that act as active adsorption sites. A lower Si/Al ratio leads to a greater number of adsorption sites per unit mass, thereby enhancing CO_2 adsorption capacity. Additionally, silicoaluminate zeolites contain Lewis base sites originating from oxygen atoms adjacent to aluminum. As aluminum content increases, the density of these basic sites also rises, strengthening interactions with acidic CO_2 molecules and improving adsorption efficiency (Barthomeuf, 1984).

However, the Si/Al ratio also affects the available pore volume, as each aluminum site requires a charge-balancing cation. In zeolites with a low Si/Al ratio, the abundance of cations per unit mass can create steric hindrance, potentially limiting the accessible pore space and reducing overall adsorption capacity.

2.4.3 Extra-framework Cations

The adsorption properties of zeolites can be tailored by exchanging extra-framework cations, typically Na^+, with other mono- or multivalent cations. This cation substitution influences the acid–base characteristics of the zeolite. The acidic sites are associated with the exchangeable cations, while the basic sites correspond to oxygen atoms bonded to aluminum within the framework (Barthomeuf, 2003). The strength of these basic sites increases as the electronegativity of the cation decreases, as a less electronegative cation enhances the negative charge on the oxygen atoms in the zeolite framework.

The basicity of zeolites exchanged with alkali cations follows the order: Cs^+ > Rb^+ > K^+ > Na^+ > Li^+. Zeolites with higher basicity exhibit stronger interactions with acidic CO_2, leading to enhanced adsorption capacity and selectivity. Furthermore, as the ionic radius increases (Li^+ < Na^+ < K^+ < Rb^+ < Cs^+), the polarizing power of the cations decreases, weakening interactions with CO_2 for larger cations.

2.4.4 Diffusion of Adsorbates through the Zeolite Frameworks

The diffusion rate of adsorbates via zeolite pores is crucial for achieving rapid adsorption equilibrium. Additional factors that significantly impact the diffusion of adsorbates through zeolite pores include partial blockage of micropores by cations and the interaction between the adsorbate and these cations (Boer et al., 2023).

2.4.5 Influence of Water

In zeolites A and zeolite X, the CO_2 adsorption capacity could be reduced significantly by the presence of small amounts of water vapor. The reduction is due to competition between CO_2 and H_2O for the same adsorption sites, with H_2O strongly interacting with the zeolite's sites due to its dipole moment.

CHAPTER III

EXPERIMENTAL

3.1 Materials and methods

3.1.1 Materials

Silica gel was collected from desiccant packets in furniture boxes. Its silica purity analyzed by energy dispersive X-ray fluorescence (EDXRF, Horiba, XGT-5200) was 99%. It was dissolved in sodium hydroxide (NaOH) solution and used as a silica source. Zeolite NaA, NaX and NaY were synthesized according to the methods from the literature (Jantarit et al., 2020; Keawkumay et al., 2019; Khaosomboon et al., 2018).

3.1.2 Synthesis of zeolite A by using silica gel waste

Zeolite NaA was prepared through hydrothermal method with an overall gel composition of $3.165Na_2O$: Al_2O_3: $1.926SiO_2$: $128H_2O$ (Khaosomboon et al., 2018).

NaOH (12.27 g) was dissolved in distilled water (90 mL) in a Teflon bottle under stirring. The solution was then split into two equal parts: one portion remained in the original beaker, while the other was transferred to a separate Teflon bottle.

In the Teflon bottle, silica gel waste (2.04 g) was introduced, and the mixture was stirred at 90 °C for 3 h. Meanwhile, in the beaker, anhydrous $NaAlO_2$ (6.36 g) was introduced and stirred at room temperature until a clear solution formed. The aluminate solution was then rapidly combined with the silicate solution, resulting in the formation of a thick gel. The container was sealed, and the mixture was stirred at room temperature for 30 min until homogeneous.

The overall gel was crystallized through the hydrothermal method at 80 °C for 2.5 h under static conditions. Once cooled, the sample was repeatedly washed with distilled. Finally, the samples were dried overnight at 90 °C.

3.1.3 Synthesis of zeolite X by using silica gel waste as silica source

Zeolite NaX was prepared through hydrothermal method with an overall gel composition of Na_2O: $4Al_2O_3$: $16SiO_2$: $325H_2O$ (Jantarit et al., 2020).

The sodium silicate solution was prepared from silica gel waste. First, NaOH (4.83 g) was dissolved in distilled water (26.67 g) in a Teflon bottle under stirring. Then, silica gel waste (12.3 g) was added slowly, and the mixture was stirred at room temperature for 18 h.

A solution was prepared by dissolving NaOH (27.24 g) in distilled water (264 g) in a Teflon bottle and stirring until fully dissolved. Then, anhydrous $NaAlO_2$ (4.08 g) was added, and the mixture was stirred at room temperature for 1 h. After that, sodium silicate solution was added and stirred for another hour until homogeneous.

The overall gel was crystallized by hydrothermal at 90 °C for 18 h. After cooling, the samples were washed with distilled water until the filtrate's pH was below 7, using multiple centrifugation cycles at 4000 rpm for 5 min each. Finally, the samples were dried overnight at 90 °C

3.1.4 Synthesis of zeolite Y by using silica gel waste as silica source

Zeolite NaY was prepared through hydrothermal method with an overall gel composition of $4.62Na_2O$: Al_2O_3: $10SiO_2$: $180H_2O$ (Keawkumay et al., 2019).

The sodium silicate solution was prepared from silica gel waste by dissolving NaOH (11.5 g) in distilled water (59.8 g) in a Teflon bottle and stirring until a clear solution was obtained. Then, silica gel waste (28.7 g) was slowly added, and the mixture was stirred at room temperature for 24 h.

A seed gel was prepared by dissolving NaOH (1.02 g) in distilled water (5.1 g) in a Teflon bottle and stirring until a clear solution was obtained. Then, anhydrous $NaAlO_2$ (0.52 g) was added and stirred until homogeneous. After that, Na_2SiO_3 solution (5.66 g) was added, and the mixture was stirred for 10 min, capped, and aged at room temperature for 24 h.

A feedstock gel was prepared from NaOH (0.035 g) dissolved in distilled water (32.74 g) in a plastic beaker, followed by adding anhydrous $NaAlO_2$ (3.27 g). The mixture was stirred until homogeneous. Then, Na_2SiO_3 solution (35.61 g) was added and stirred vigorously for 10 min.

The feedstock gel was then added into the seed gel, stirred for 10 min, sealed, and aged for 24 h at room temperature. The overall gel was crystallized using the hydrothermal method at 90 °C for 24 h. After cooling, the white precipitate was washed

repeatedly with distilled water until the filtrate's pH was below 9, using multiple centrifugation cycles at 4000 rpm for 5 min. Finally, the product was dried overnight at 90 °C.

3.2 Spectroscopic measurement

The elemental compositions of the products were determined using a wavelength-dispersive X-ray fluorescence spectrometer. The X-ray source was an Rh X-ray tube with a collimator size of 150 μm. A sample holder with an optical path diameter of 37 mm was used for measurement. The X-ray generator was operated at 50 kV and 60 mA.

The identity of the zeolite products was confirmed using X-ray diffraction (XRD) on a Bruker D8 ADVANCE with a monochromatic Cu K_α radiation source (λ = 1.5418 Å), operated at 40 kV and 40 mA. The samples were analyzed over a 2θ range of 5–50° with a scan speed of 0.2 s/step and an increment of 0.02 °/step.

The morphology of the zeolites was characterized using scanning electron microscopy (SEM-EDX, JEOL JSM-6400) with an accelerating voltage of 20 kV, a vacuum pressure of 10^{-4} Pa, and a tungsten filament. The synthesized samples were spread on carbon tape and coated with gold or carbon. The particle size of the zeolite was analyzed from SEM images using ImageJ software along the X-axis (horizontal), Y-axis (vertical), and Z-axis (depth), with at least three measurements per sample.

The zeolites' functional groups were analyzed using Fourier transform infrared spectroscopy (FTIR) on a Bruker Vertex 70 + RamII FTIR spectrometer in attenuated total reflectance (ATR) mode. The measurements were performed with a resolution of 4 cm^{-1}.

The N_2 adsorption–desorption analysis was performed on a Micromeritics ASAP 2010 analyzer over a relative pressure range of 0.01 to 0.99. Prior to measurement, the zeolite samples were degassed under vacuum at 300 °C for 8 h. Surface areas were determined using the Brunauer-Emmett-Teller (BET) method, while external surface areas, micropore areas, and micropore volumes were calculated using the t-plot method.

CO_2 temperature-programmed desorption (CO_2-TPD) was conducted using a BEL-CAT B chemisorption analyzer to determine the basicity of each adsorbent. Each sample (0.050 g) was placed in a quartz U-tube reactor, pretreated at 500 °C for 3 h under a helium flow of 50 mL/min, and then cooled to 70 °C while maintaining the helium flow. The system was then exposed to 10% CO_2 diluted in helium at a total flow rate of 50 mL/min for 30 min to allow adsorption.

Next, the sample was heated to 100 °C, and purged for 1 h to remove physisorbed CO_2. Finally, the temperature was ramped at a rate of 10 °C/min from 100 °C to 800 °C. The amount of CO_2 absorbed (in mmol of CO_2) was determined online using a thermal conductivity detector (TCD) by comparing the peak area with a calibration curve obtained from a known amount of CO_2 in the injection loop.

The basicity in mmol CO_2 $g_{adsorbent}^{-1}$ was calculated by

$$\text{Basicity (mmol } CO_2 \text{ } g^{-1}) = \frac{CO_2 \text{ adsorbed of sample (mmol)}}{\text{sample weight (g)}}$$

CO_2 adsorption experiments was performed with a method from the literature (Keawkumay et al., 2024). Samples were degassed under vacuum at 300 °C for 3 h to remove adsorbed molecules. Adsorption measurements were conducted at 25 °C over a pressure range of 0–100 kPa using a Quantachrome Autosorb IQ3. Adsorption isotherms were obtained by plotting the amount of CO_2 adsorbed against pressure. The CO_2 adsorption capacity (mmol/g) for each sample was calculated at 100 kPa and 25 °C by converting the adsorbed CO_2 volume to mmol.

3.3 Adsorption equilibrium isotherm equations

This study utilizes four models to investigate the adsorbate-adsorbent interactions: Langmuir, Freundlich, Langmuir-Freundlich (Sips) and Toth models.

The Langmuir model assumes that adsorption takes place at specific, uniform sites on the surface of an adsorbent. Once a site is occupied by an adsorbate, no additional adsorption can occur at that same location.

$$\frac{C_e}{q_e} = \frac{1}{K_L q_m} + \frac{1}{q_m} C_e$$

where, q_m (mg g^{-1}) is the theoretical maximum adsorption capacity, K_L (L mg^{-1}) is the Langmuir isotherm constant, C_e is the equilibrium concentration (mg L^{-1}).

The Freundlich equation models a non-linear adsorption process over a range of adsorbate concentrations and effectively describes adsorption on surface sites with heterogeneous energy levels.

$$\ln q_e = \frac{1}{n} \ln C_e + \ln K_f$$

where, K_f (L mg^{-1}) and n represent the Freundlich isotherm constant and heterogeneity factor, respectively.

The Toth isotherm model is a useful modification of the Langmuir model, improving the accuracy of predicted values compared to experimental results by considering sub monolayer coverage. It is used to describe adsorption on heterogeneous surfaces across a wide range of adsorbate concentrations.

$$q_e = \frac{q_m K_T C_e}{[1+(K_T C_e)^{n_T}]^{\frac{1}{n_T}}}$$

where, q_m repesent maximum adsorption capacity (mmol g^{-1}), K_T is Toth isotherm constant (bar^{-1}), n_T is heterogeneity factor (–). If the surface is homogenous, then n_T equals one, indicating that there is no difference in the relative energies of the various adsorption sites.

The Sips isotherm model (Langmuir-Freundlich) is a hybrid of the Langmuir and Freundlich model equations. It was created to predict heterogeneous adsorption systems while overcoming the limitations associated with increasing adsorbate concentrations that arise with the Freundlich isotherm model. Consequently, at low adsorbate concentrations, this model aligns with the Freundlich isotherm, while at

high concentrations, it predicts monolayer adsorption, characteristic of the Langmuir isotherm.

$$q_e = \frac{q_m (K_s C_e)^{\frac{1}{n_S}}}{1 + (K_s C_e)^{\frac{1}{n_S}}}$$

where, q_m is maximum adsorption capacity (mmol g^{-1}), K_s is Sips isotherm constant (bar^{-1}), and n_s is Sips isotherm exponent (–).

CHAPTER IV
RESULTS AND DISCUSSION

4.1 Chemical compositions of silica gel waste

The chemical components of silica gel waste in the form of stable oxides are shown in Table 3. The major component was SiO_2, along with small amounts of other inorganic oxides, including Na_2O, MgO, TiO_2, CaO, and Fe_2O_3. Furthermore, the amorphous-phase silica obtained could be advantageous for zeolite synthesis, as it dissolves easily in NaOH solution to yield sodium silicate (Na_2SiO_3) (Keawkumay et al., 2024).

Table 3 Elemental composition of silica gel waste determined by XRF analysis.

Sample	Component (wt%)					
	SiO_2	Na_2O	MgO	TiO_2	CaO	Fe_2O_3
Silica gel waste	95.96	1.86	1.36	0.33	0.23	0.27

4.2 Characterization of synthesized zeolites

The SEM images in Figure 7 illustrate the morphologies of six zeolite samples, including synthesized and commercial forms of Zeolite A, X, and Y, all synthesized using silica gel waste as a silica source. Zeolite A, shown in images (a) and (d), exhibits a well-defined cubic morphology with smooth surfaces and sharp edges, indicative of high crystallinity. The synthesized zeolite A (a) consists of smaller, uniform cubic crystals with a size of 0.46 ± 0.041 μm, whereas the commercial zeolite A (d) features larger, more distinct cubic structures with a size of 2.0 ± 0.13 μm.

Zeolite X, presented in images (b) and (e), exhibits a polycrystalline structure with intergrown crystallites forming aggregated particles. The synthesized zeolite X (b) has a rough and irregular morphology, with a shape resembling a Takraw ball, where the crystallites appear interwoven and interconnected, with a size of 1.1 ± 0.10 μm.

In contrast, the commercial zeolite X (e) consists of more well-defined and larger crystals, some showing partially truncated octahedral shapes, with a size of 2.2 ± 0.24 μm.

Zeolite Y, shown in images (c) and (f), has a highly porous and loosely packed morphology. The synthesized zeolite Y (c) consists of fine, irregularly aggregated particles with a size of 0.14 ± 0.019 μm, whereas the commercial zeolite Y (f) displays larger, fragmented crystals with a rough and textured surface, measuring 0.62 ± 0.041 μm. These differences in morphology and particle size between the synthesized and commercial samples indicate variations in crystallization conditions, degree of crystallinity, and structural purity.

XRD patterns of synthesized and commercial zeolite A, X, Y are shown in Figure 8. Main peaks of zeolite A, X, Y were similar to those of the commercial zeolites indicating zeolites is pure phase. Then, XRD patterns of pure-phase zeolite NaX on the diffraction peaks at 2θ ~ 7° are impurity phases. Then, the XRD pattern of synthesized zeolite Y represents the low peak intensity, which indicates low crystallinity compared with commercial zeolite Y. Low crystallinity suggests incomplete growth or poor ordering of the crystalline. The results indicated that silica gel waste can be used as a precursor in the synthesis of phase-pure zeolite A, X, Y.

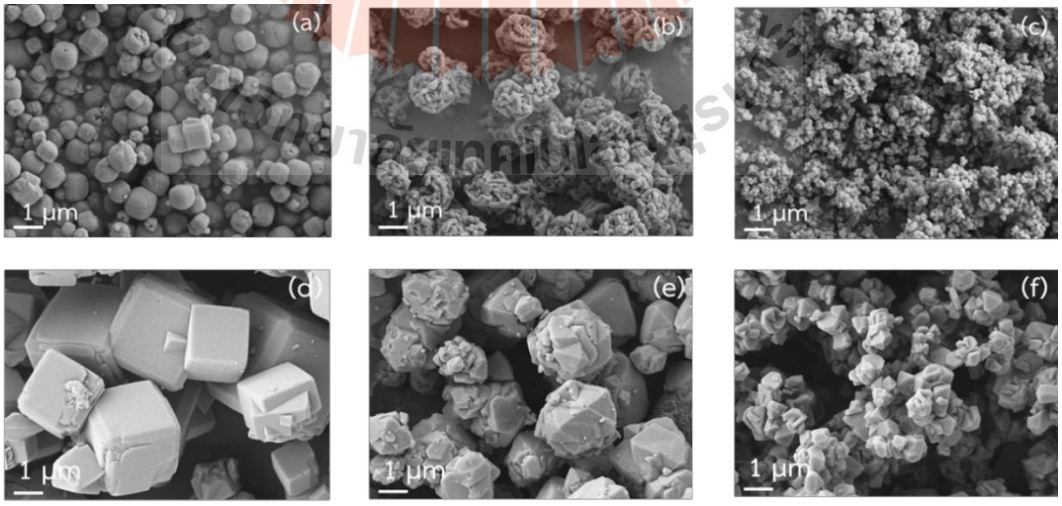

Figure 7 SEM image of synthesized zeolite A (a), synthesized zeolite X (b), synthesized zeolite Y (c), commercial A (d), commercial X (e), and commercial Y (f) by using silica gel waste as silica source with a magnification of 10 KX.

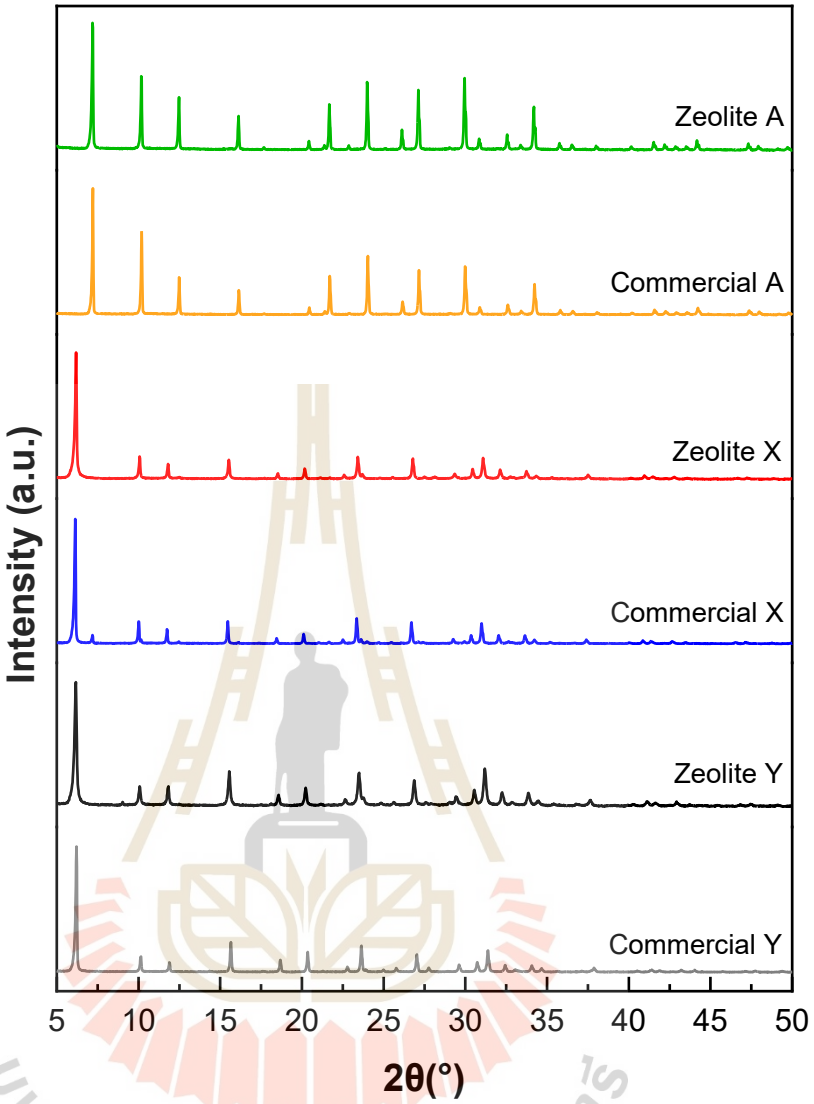

Figure 8 XRD pattern of synthesized and commercial zeolites.

FTIR spectra were recorded in the 400–4000 cm^{-1} range to identify the vibrational functional group vibrations in the zeolite structure. The spectra of the synthesized zeolite and commercial NaA, NaX, and NaY are presented in Figure 9. The bands corresponding to the internal deformation vibration modes of T-O-T bridges (where T = Si, Al) and the internal T-O symmetric stretching vibrations are only slightly affected by the Si/Al ratio. Transmittance peaks were observed at 465 and 663 cm^{-1} for zeolite NaA, and at 453 and 669 cm^{-1} for zeolite NaX, respectively. The band corresponding to the asymmetric external vibration of the double four-rings in the zeolite framework is more sensitive to the Si/Al ratio, appearing at 550 cm^{-1} for zeolite

NaA and at 561 cm^{-1} for zeolite NaX. The T–O–T vibration band gives a peak at 748 cm^{-1}, observed only for zeolite NaX. The internal T-O asymmetric stretching vibration produces peaks at 987 cm^{-1} for zeolite NaA and at 976 cm^{-1} for zeolite NaX. In both spectra, bands around 1640 and 3370 cm^{-1} are observed, corresponding to the presence of H_2O and hydroxyl groups, respectively. These FTIR bands are consistent with those previously reported for zeolite A and zeolite X (Keawkumay et al., 2024; Tsitsishvili, 2019).

The synthesized zeolite NaY exhibits six prominent peaks characteristic of the zeolite NaY framework. The band at 566 cm^{-1} corresponds to the double-ring vibration characteristic of the FAU zeolite framework. The band at 993 cm^{-1} is assigned to asymmetric and symmetric stretching vibrations of Si–O–Si, Si–O–Al, and O–Al–OH within the internal TO_4 structure (T = Si, Al). The bands at 1146 and 770 cm^{-1} are attributed to the asymmetric and symmetric stretching vibrations of the external TO_4 structure (T = Si, Al), respectively. The band at 1390 cm^{-1} is attributed to the double-ring external linkage associated with the FAU structure. The band at 3420 cm^{-1} corresponds to Si–OH, Si–OH–Al, and OH hydroxyl groups (Mekki et al., 2020). The characteristic bands of the zeolite NaY sample are weaker compared to those of the other materials, indicating a decrease in crystallinity, which aligns with the XRD analysis results. Furthermore, the FTIR patterns of the synthesized zeolite samples closely resemble those of the commercial zeolites. This result suggests that the zeolite synthesized from silica gel waste has a zeolite phase.

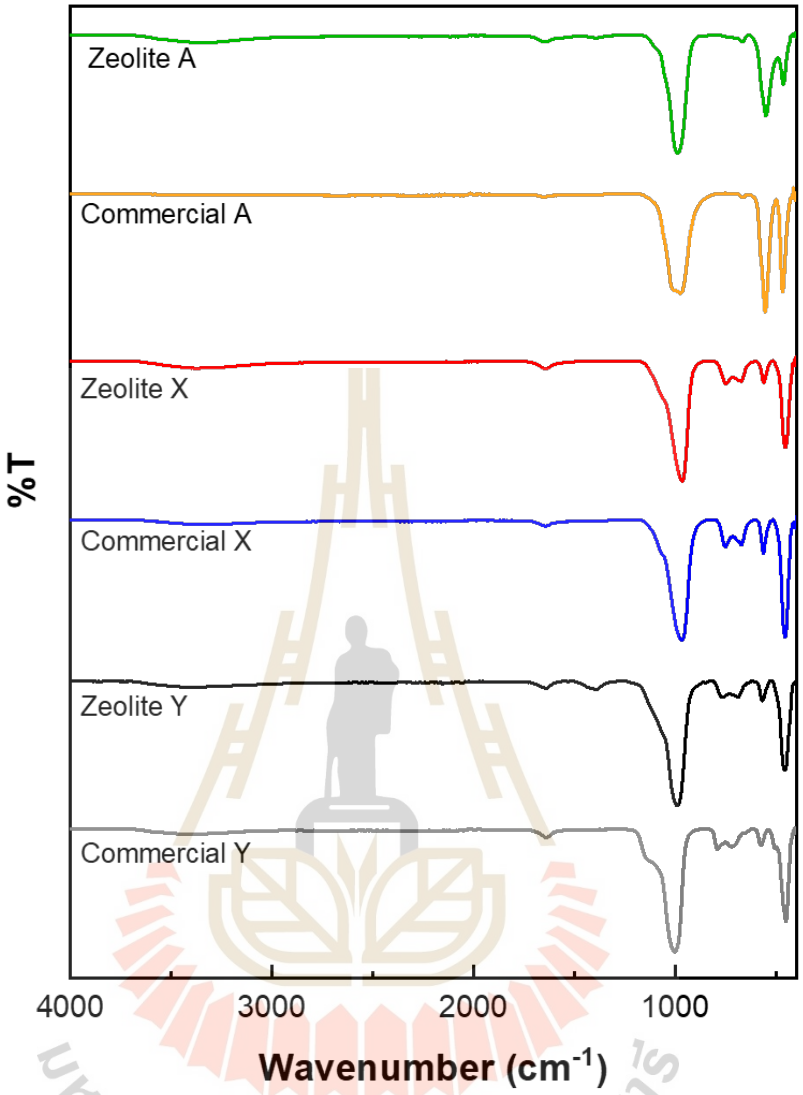

Figure 9 FTIR spectra synthesized and commercial zeolites.

Figure 10 shows the SEM-EDS mapping of NaA, NaX, and NaY zeolites, illustrating the elemental distribution of Al, Si, O, and Na across the zeolite particles. The Si/Al ratios are presented in Table 4.

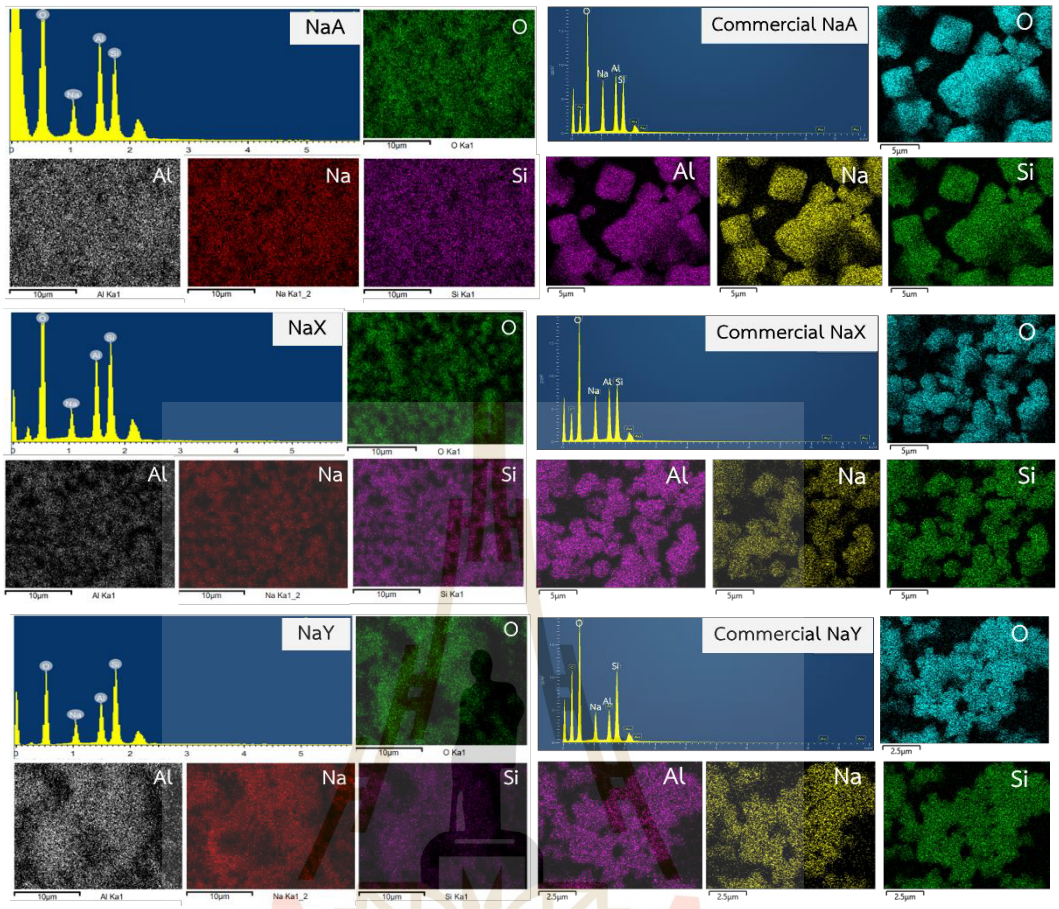

Figure 10 SEM-EDS mapping of synthesized and commercial NaA, NaX and NaY.

Table 4 Synthesis gel composition and Si/Al ratio of the zeolite products.

Sample	Synthesis gel composition			Si/Al ratio[a]	Si/Al ratio[b]
	$NaOH/SiO_2$	SiO_2/Al_2O_3	H_2O/SiO_2		
Zeolite A	10	0.5	145	1.01±0.010	1.17±0.024
Zeolite X	4	4	22	1.46±0.033	1.67±0.023
Zeolite Y	0.462	10	18	2.11±0.155	2.25±0.007

[a]SEM-EDS

[b]ED-XRF

Figure 11 displays the N_2 adsorption–desorption isotherms of all zeolites. Both the synthesized and commercial zeolites exhibit Type I(a) isotherms, characteristic of microporous materials with predominantly narrow micropores (< ~1 nm). The steep

uptake at low P/P_0 reflects micropore filling due to strong adsorbent-adsorptive interactions, with adsorption capacity primarily determined by micropore volume rather than surface area. Additionally, the presence of H4 hysteresis at $P/P_0 > 0.4$ indicates the coexistence of mesopores (2–50 nm) alongside micropores, while the pronounced uptake at low P/P_0 corresponds to micropore filling (Thommes et al., 2015).

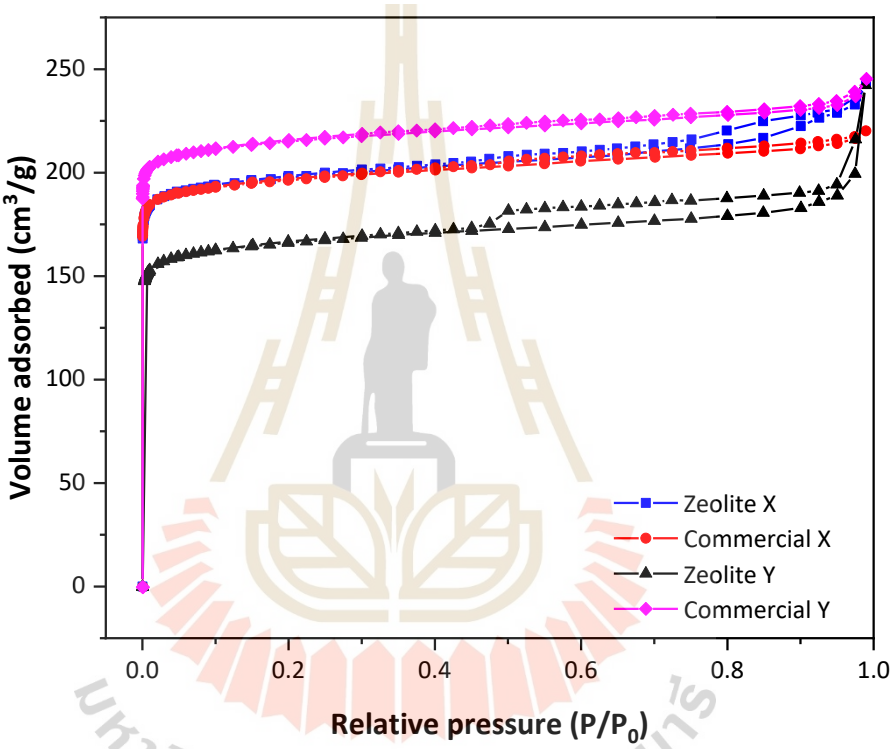

Figure 11 N_2 adsorption–desorption isotherms of zeolite NaA, zeolite NaX and zeolite NaY using silica gel waste as silica source.

Table 5 summarizes the BET surface area, external surface area, micropore surface area, and micropore volume of the synthesized and commercial zeolites. The surface area of the synthesized NaX was comparable to that of the commercial NaX, while the synthesized NaY exhibited a significantly lower surface area than its commercial counterpart. This difference is attributed to the lower crystallinity of the synthesized NaY, which leads to structural defects and a non-uniform pore distribution. These defects likely result in gaps or voids between particles, forming

interparticle voids or mesopores, ultimately reducing the overall surface area (Yates, 1968).

Table 5 Surface area of Synthesized Zeolites Determined from N_2 Adsorption–Desorption Isotherms.

Samples	Surface area[a] (m^2/g)	External surface area[b] (m^2/g)	Micropore surface area[b] (m^2/g)	Micropore volume[b] (cm^3/g)
Zeolite X	800	58	744	0.27
Commercial X	800	41	759	0.28
Zeolite Y	669	54	615	0.23
Commercial Y	876	42	835	0.30

[a]BET method

[b]*t*-plot method

Figure 12 presents the CO_2-TPD profiles of synthesized and commercial zeolites, showing two desorption temperature regions: 150-300 °C, corresponding to weak and medium basic sites, and above 300 °C, indicating strong basic sites. The corresponding basicity of each sample is summarized in Table 6. CO_2-TPD was used to evaluate the strength of basic sites in zeolites for CO_2 adsorption. The basicity follows the order: Commercial A > Zeolite A > Commercial X > Zeolite X > Commercial Y > Zeolite Y. The variation in basic site strength correlates with the Si/Al ratio and pore sizes of zeolites. A lower Si/Al ratio in zeolite NaA results in a higher incorporation of aluminum atoms into the framework, increasing the density of negatively charged sites AlO_4^-, which enhanced basicity. In contrast, the larger pores of NaX and NaY facilitate easier diffusion CO_2 molecules, leading to weaker interactions with the zeolite surface. As a result, CO_2 desorption requires less energy, manifesting as lower desorption temperatures and reduced basic site strength.

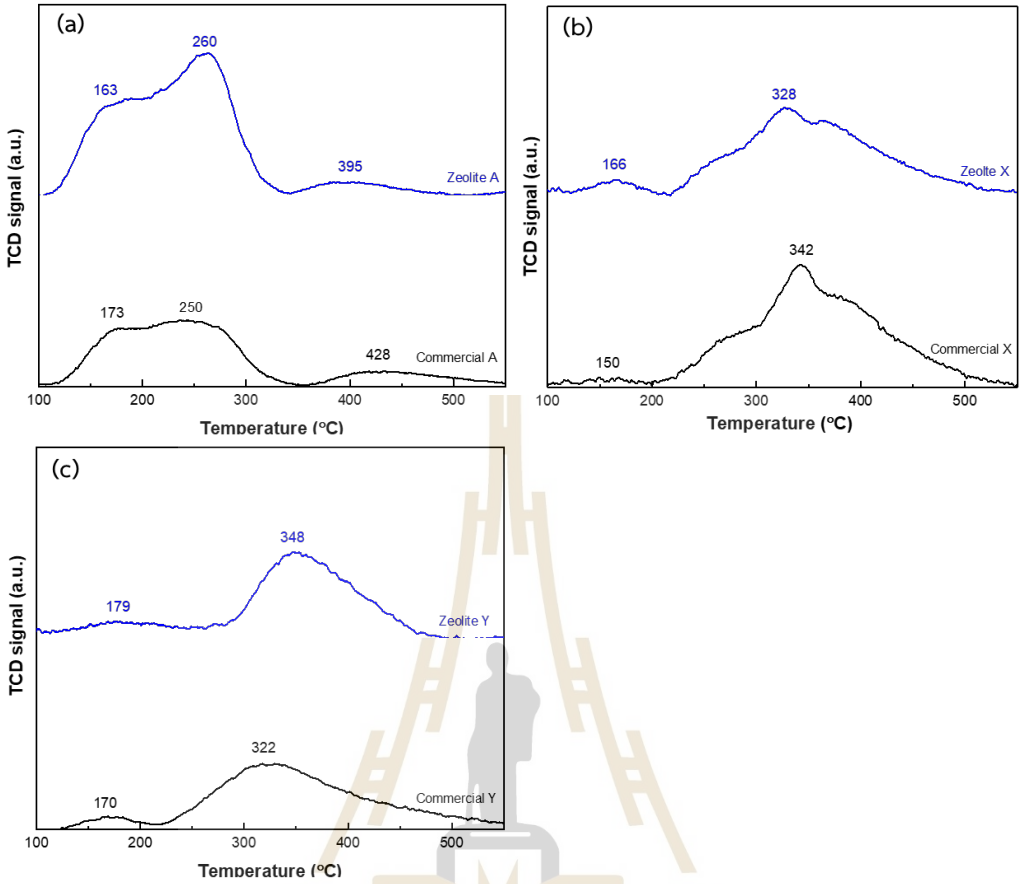

Figure 12 CO_2-TPD profiles of synthesized and commercial NaA (a), synthesized and commercial NaX (b) and synthesized and commercial NaY (c).

Table 6 Basicity of synthesized and commercial zeolites.

Samples	Basicity (mmol g^{-1})
Zeolite A	0.135
Commercial A	0.139
Zeolite X	0.052
Commercial X	0.068
Zeolite Y	0.037
Commercial Y	0.039

4.3 CO_2 adsorption capacity

Figure 13 displays the CO_2 adsorption isotherms of NaA, NaX, NaY, and their commercial counterparts. According to the IUPAC classification, all isotherms are Type

I, indicating monolayer adsorption. The isotherms exhibit a sharp uptake at low pressure due to the abundance of adsorption sites, followed by a gradual decline in adsorption rate before stabilizing at higher pressures. The adsorption behavior remains stable near 1 bar.

The primary interactions between zeolites and CO_2 molecules are predominantly electrostatic. Zeolites adsorb CO_2 through strong quadrupolar interactions between the adsorbate molecules and the electric field generated by the charge-balancing cations within the zeolite cavity. The type and spatial distribution of these cations (e.g., Na^+) influence the strength and uniformity of the electric field, thereby affecting adsorption behavior. At low pressures, CO_2 uptake increases significantly due to the availability of accessible cations in the zeolite cavities. However, at higher relative pressures, once all cations are occupied, the adsorption curve plateaus, indicating a nearly constant adsorption capacity (Bonenfant et al., 2008; Keawkumay et al., 2024; Siriwardane et al., 2005).

The CO_2 adsorption capacity followed the order: zeolite NaX > commercial NaX > commercial NaY > zeolite NaY > Commercial NaA > zeolite NaA. This trend strongly correlates with the total number of basic sites (Table 6) and the structural properties of the zeolites. Silicoaluminate zeolites also contain Lewis base sites, which originate from oxygen atoms adjacent to aluminum. The zeolite framework consists of tetrahedral TO_4 units (T = Si or Al) interconnected through shared oxygen atoms, generating a net negative charge. This charge is balanced by sodium ions (Na^+) (Salehi and Anbia, 2017). Both a net negative charge and the presence of Na^+ serve as active sites for CO_2 adsorption.

Zeolites with lower Si/Al ratios have a higher aluminum content, resulting in an increased number of extra-framework cations and basic sites. These active sites can interact with the acidic CO_2 molecule, leading to zeolites with lower Si/Al ratios exhibiting greater adsorption capacity and selectivity for CO_2 (Abdullahi et al., 2017). Thus, from these results, zeolite NaX shows higher adsorption capacity than the zeolite NaY (5.84 vs. 4.39 mmol g^{-1} in Table 7).

The lower CO_2 adsorption capacity of synthesized zeolite A compared to zeolite X is attributed to differences in their structural properties. Zeolite X has larger

pores (~7.4 Å) than zeolite A (~4.1 Å), allowing faster CO_2 diffusion through the pores and better access to adsorption sites, thereby enhancing adsorption capacity. In contrast, the smaller, more restrictive pores of zeolite A hinder CO_2 diffusion, limiting access to internal adsorption sites and reducing its adsorption capacity.

The synthesized NaY zeolite exhibited lower CO_2 adsorption capacity than commercial NaY, primarily due to differences in crystallinity. Since CO_2 adsorption depends on crystallinity, the reduced surface area and pore volume of synthesized NaY, resulting from lower crystallinity, led to decreased adsorption (Table 5). Conversely, the synthesized NaX samples demonstrated higher adsorption capacity than their commercial counterparts, likely due to the presence of impurity phases in commercial NaX, which negatively affect adsorption performance.

These findings confirm that zeolites synthesized from silica gel waste are effective CO_2 adsorbents due to their high adsorption capacity and straightforward synthesis process. Moreover, utilizing silica gel waste as a silica source presents a cost-effective and environmentally sustainable approach with significant potential for scalable production.

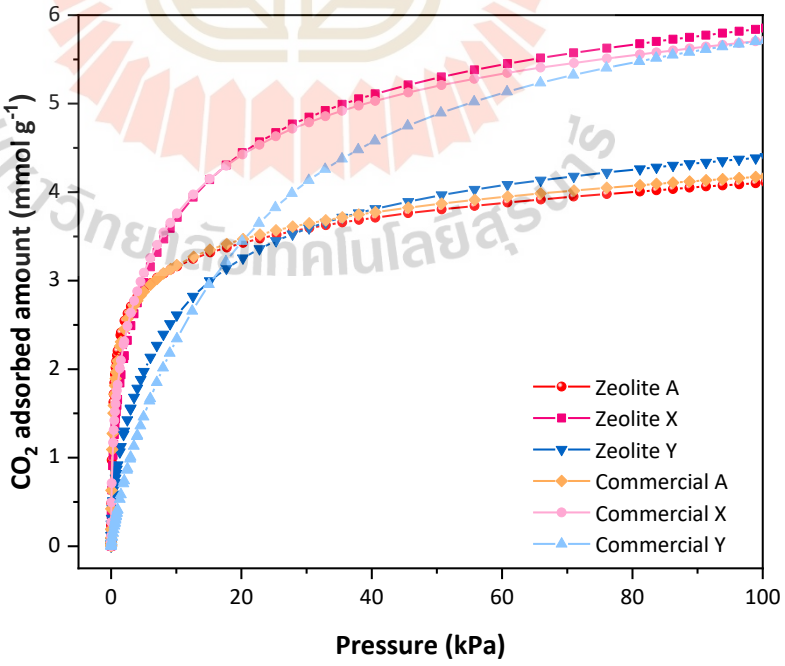

Figure 13 CO_2 adsorption isotherms of synthesized zeolites and commercial zeolites performed at 25 °C and the pressure range of 0–100 kPa.

Table 7 CO_2 adsorption capacity from synthesized and commercial zeolites.

Sample	CO_2 adsorption capacity	
	(mg g^{-1})	(mmol g^{-1})
Zeolite NaA	180	4.10
Zeolite NaX	257	5.84
Zeolite NaY	193	4.39
Commercial NaA	183	4.17
Commercial NaX	251	5.70
Commercial NaY	251	5.70

4.4 CO_2 adsorption isotherm

Figure 14 presents the CO_2 adsorption isotherm fitting with Langmuir, Freundlich, Langmuir-Freundlich, and Toth models. The correlation coefficient (R^2) values from each model from all samples are summarized in Table 8. The results indicate that CO_2 adsorption in both synthesized and commercial zeolite NaA fits well with the Toth isotherm, achieving an R^2 value greater than 0.999, better than Langmuir, Freundlich, and Langmuir-Freundlich models.

For synthesized and commercial NaX and NaY zeolites, the Sips adsorption model provided the best fit for CO_2 adsorption. A higher R^2 value signifies greater applicability and reliability of the corresponding model. These results are in good agreement with previous studies in the literature (Cui et al., 2023; Keawkumay et al., 2024; Zouaoui et al., 2021).

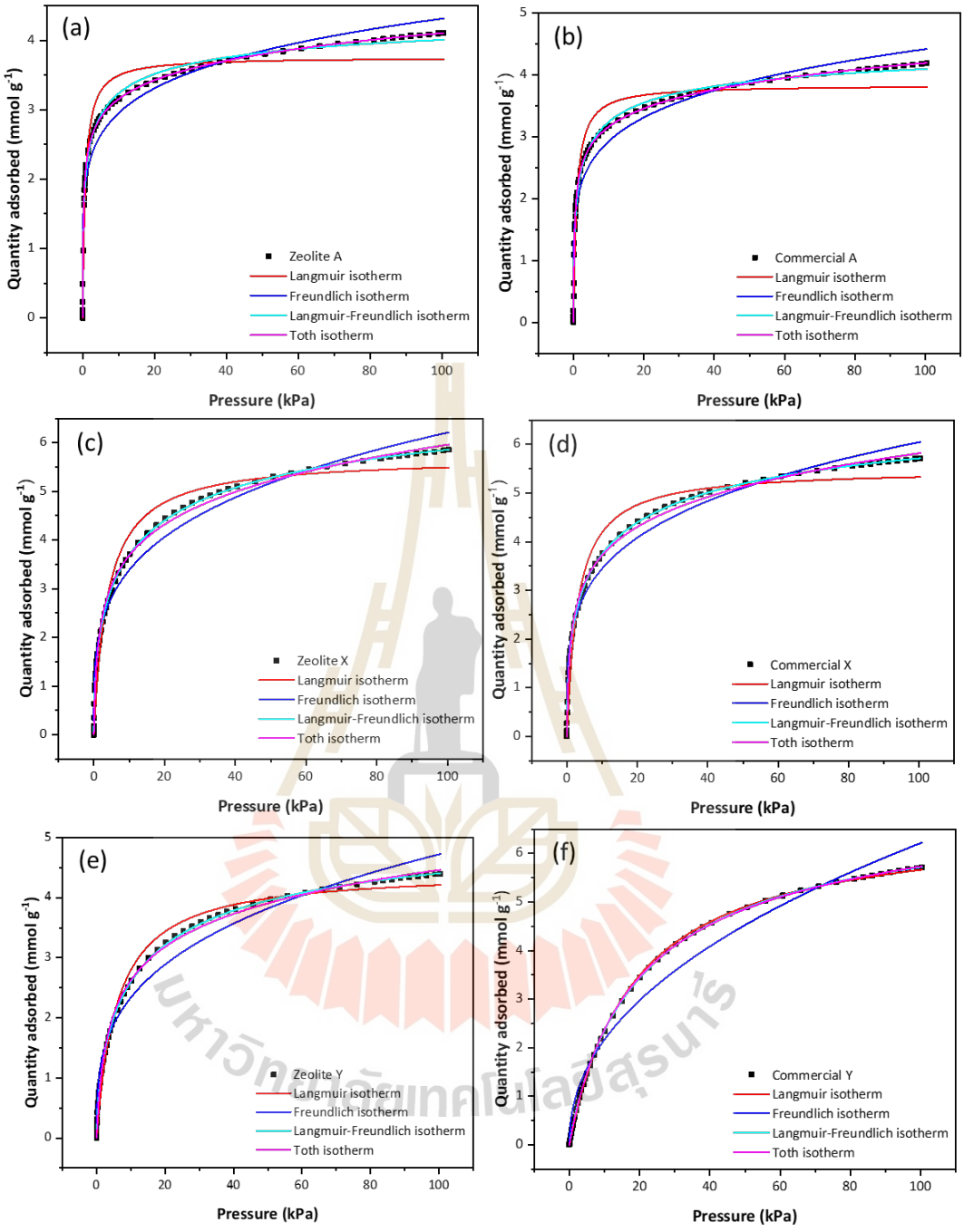

Figure 14 CO_2 adsorption isotherms of NaA (a), Commercial NaA (b), NaX (c), Commercial NaX (d), NaY (e) and commercial NaY (f) fitted with Langmuir, Freundlich, Langmuir-Freundlich and Toth models.

Table 8 Correlation coefficient (R^2) values from CO_2 adsorption isotherm of commercial and synthesized zeolites.

Samples	Correlation coefficients (R^2)			
	Langmuir	Freundlich	Langmuir-Freundlich	Toth
Zeolite NaA	0.95904	0.95622	0.99639	0.99910
Zeolite NaX	0.97434	0.98308	0.99984	0.99749
Zeolite NaY	0.98792	0.97886	0.99962	0.99747
Commercial NaA	0.96043	0.95973	0.99748	0.99952
Commercial NaX	0.96879	0.98259	0.99982	0.99762
Commercial NaY	0.99952	0.97746	0.99997	0.99984

CHAPTER V
CONCLUSIONS

Pure-phase zeolites A, X, and Y in sodium forms were successfully synthesized from silica gel waste by the conventional hydrothermal method. The synthesized zeolites demonstrated excellent CO_2 adsorption capacities, achieving 4.10 mmol/g for NaA, 5.84 mmol/g for NaX, and 4.39 mmol/g for NaY. Notably, the synthetic NaX zeolite exhibited a higher adsorption capacity (5.84 mmol/g) compared to its commercial counterpart (5.70 mmol/g). The CO_2 adsorption behavior of both synthesized and commercial NaA zeolites is well-described by the Toth model. Meanwhile, the Langmuir-Freundlich adsorption model provided the best fit for CO_2 adsorption in both synthesized and commercial NaX and NaY zeolites. These results demonstrate that zeolites synthesized from silica gel waste are highly effective for CO_2 capture.

REFERENCES

REFERENCES

Abdullahi, T., Harun, Z., and Othman, M. H. D. (2017). A review on sustainable synthesis of zeolite from kaolinite resources via hydrothermal process. *Advanced Powder Technology, 28*(8), 1827-1840.

Amoni, B. d. C., Freitas, A. D. L. d., Loiola, A. R., Soares, J. B., and Soares, S. d. A. (2019). A method for NaA zeolite synthesis from coal fly ash and its application in warm mix asphalt. *Road Materials and Pavement Design, 20*(sup2), S558-S567.

Bakkali, F., Averbeck, S., Averbeck, D., and Idaomar, M. (2008). Biological effects of essential oils-a review. *Food and chemical toxicology, 46*(2), 446-475.

Barthomeuf, D. (1984). Conjugate acid-base pairs in zeolites. *The Journal of Physical Chemistry, 88*(1), 42-45.

Barthomeuf, D. (2003). Framework induced basicity in zeolites. *Microporous and Mesoporous Materials, 66*(1), 1-14.

Boer, D. G., Langerak, J., and Pescarmona, P. P. (2023). Zeolites as selective adsorbents for CO_2 separation. *ACS Applied Energy Materials, 6*(5), 2634-2656.

Bonenfant, D., Kharoune, M., Niquette, P., Mimeault, M., and Hausler, R. (2008). Advances in principal factors influencing carbon dioxide adsorption on zeolites. *Science and technology of advanced materials, 9*(1), 013007.

Cholmaitri, C., Uthairatanakij, A., Laohakunjit, N., Jitareerat, P., and Mingvanish, W. (2020). Controlled release of methyl salicylate by biosorbents delays the ripening of banana fruit. *PeerJ Materials Science, 2*, e12.

Costa, S. P., Soares, O. v. S., Aguiar, C. A., and Neves, I. C. (2022). Fragrance carriers obtained by encapsulation of volatile aromas into zeolite structures. *Industrial Crops and Products, 187*, 115397.

Cui, Y., Xing, Y., Tian, J., Su, W., Sun, F.-Z., and Liu, Y. (2023). Insights into the adsorption performance and separation mechanisms for CO_2 and CO on NaX and CaA zeolites by experiments and simulation. *Fuel, 337*, 127179.

Dasgupta, A., Wahed, A., Dasgupta, A., and Wahed, A. (2014). Common poisonings including heavy metal poisoning. *Clinical Chemistry, Immunology and Laboratory Quality Control*, 337-351.

Davarpanah, E., Armandi, M., Hernández, S., Fino, D., Arletti, R., Bensaid, S., and Piumetti, M. (2020). CO_2 capture on natural zeolite clinoptilolite: Effect of temperature and role of the adsorption sites. *Journal of environmental management, 275*, 111229.

de Aquino, T. F., Estevam, S. T., Viola, V. O., Marques, C. R., Zancan, F. L., Vasconcelos, L. d. B., Riella, H. G., Pires, M. a. J., Morales-Ospino, R., and Torres, A. E. B. (2020). CO_2 adsorption capacity of zeolites synthesized from coal fly ashes. *Fuel, 276*, 118143.

de Carvalho Izidoro, J., Fungaro, D. A., and Cataldo, E. (2024). Zeolites synthesized from agro-industrial residues applied in agriculture: A review and future prospects. *Soil Use and Management, 40*(1), e13003.

Evans, W., and Evans, D. (2009). Chapter 22-Volatile oils and resins. *Trease and Evans' Pharmacognosy (Sixteenth Edition): WB Saunders*, 263-303.

Gao, F., Li, Y., Bian, Z., Hu, J., and Liu, H. (2015). Dynamic hydrophobic hindrance effect of zeolite@ zeolitic imidazolate framework composites for CO_2 capture in the presence of water. *Journal of Materials Chemistry A, 3*(15), 8091-8097.

Gouveia, L. G. T., Agustini, C. B., Perez-Lopez, O. W., and Gutterres, M. (2020). CO_2 adsorption using solids with different surface and acid-base properties. *Journal of Environmental Chemical Engineering, 8*(4), 103823.

Jantarit, N., Tayraukham, P., Osakoo, N., Föttinger, K., and Wittayakun, J. (2020). Formation of EMT/FAU intergrowth and nanosized SOD zeolites from synthesis

gel of zeolite NaX containing ethanol. *Materials Research Express, 7*(7), 075011.

Kaithwas, A., Prasad, M., Kulshreshtha, A., and Verma, S. (2012). Industrial wastes derived solid adsorbents for CO_2 capture: A mini review. *Chemical Engineering Research and Design, 90*(10), 1632-1641.

Kamseu, E., á Moungam, L. B., Cannio, M., Billong, N., Chaysuwan, D., Melo, U. C., and Leonelli, C. (2017). Substitution of sodium silicate with rice husk ash-NaOH solution in metakaolin based geopolymer cement concerning reduction in global warming. *Journal of cleaner production, 142*, 3050-3060.

Keawkumay, C., Krukkratoke, P., Youngjan, S., Osakoo, N., Deekamwong, K., Khemthong, P., Phanthasri, J., Prayoonpokarach, S., and Wittayakun, J. (2024). Extraction of silica from sugarcane bagasse ash and its utilization in zeolite 4A synthesis for CO_2 adsorption. *RSC advances, 14*(27), 19472-19482.

Keawkumay, C., Rongchapo, W., Sosa, N., Suthirakun, S., Koleva, I. Z., Aleksandrov, H. A., Vayssilov, G. N., and Wittayakun, J. (2019). Paraquat adsorption on NaY zeolite at various Si/Al ratios: A combined experimental and computational study. *Materials Chemistry and Physics, 238*, 121824.

Khaleque, A., Alam, M. M., Hoque, M., Mondal, S., Haider, J. B., Xu, B., Johir, M., Karmakar, A. K., Zhou, J., and Ahmed, M. B. (2020). Zeolite synthesis from low-cost materials and environmental applications: A review. *Environmental advances, 2*, 100019.

Khaosomboon, P., Khuanmar, K., and Weerayutsil, P. (2018). Synthesis of zeolite-A and zeolite-Y using silica gel waste as silica source and modifying with Fe. *Int. J. Eng. Technol, 7*, 1376.

Khraisheh, M., Mukherjee, S., Kumar, A., Al Momani, F., Walker, G., and Zaworotko, M. J. (2020). An overview on trace CO_2 removal by advanced physisorbent materials. *Journal of environmental management, 255*, 109874.

Kuceba, I., and Nowak, W. (2005). A thermogravimetric study of the adsorption of CO_2 on zeolites synthesized from fly ash. *Thermochimica Acta, 437*(1-2), 67-74.

Lakiss, L., Gilson, J.-P., Valtchev, V., Mintova, S., Vicente, A. l., Vimont, A., Bedard, R., Abdo, S., and Bricker, J. (2020). Zeolites in a good shape: Catalyst forming by extrusion modifies their performances. *Microporous and Mesoporous Materials, 299*, 110114.

Li, Y., Yi, H., Tang, X., Li, F., and Yuan, Q. (2013). Adsorption separation of CO_2/CH_4 gas mixture on the commercial zeolites at atmospheric pressure. *Chemical Engineering Journal, 229*, 50-56.

Li, Z., Huang, J., Ye, L., Lv, Y., Zhou, Z., Shen, Y., He, Y., and Jiang, L. (2020). Encapsulation of highly volatile fragrances in Y zeolites for sustained release: Experimental and theoretical studies. *ACS omega, 5*(49), 31925-31935.

Mallard, I., Bourgeois, D., and Fourmentin, S. (2018). A friendly environmental approach for the controlled release of Eucalyptus essential oil. *Colloids and Surfaces A: Physicochemical and Engineering Aspects, 549*, 130-137.

Masoudian, S. K., Sadighi, S., and Abbasi, A. (2013). Synthesis and characterization of high aluminum zeolite X from technical grade materials. *Bulletin of Chemical Reaction Engineering & Catalysis, 8*(1), 54-60.

Maurin, G., Llewellyn, P., and Bell, R. (2005). Adsorption mechanism of carbon dioxide in faujasites: grand canonical Monte Carlo simulations and microcalorimetry measurements. *The Journal of Physical Chemistry B, 109*(33), 16084-16091.

Mekki, A., Benmaati, A., Mokhtar, A., Hachemaoui, M., Zaoui, F., Habib Zahmani, H., Sassi, M., Hacini, S., and Boukoussa, B. (2020). Michael addition of 1, 3-dicarbonyl derivatives in the presence of zeolite Y as an heterogeneous catalyst. *Journal of Inorganic and Organometallic Polymers and Materials, 30*, 2323-2334.

Muriithi, G. N., Petrik, L. F., and Doucet, F. d. r. J. (2020). Synthesis, characterisation and CO_2 adsorption potential of NaA and NaX zeolites and hydrotalcite obtained from the same coal fly ash. *Journal of CO_2 Utilization, 36*, 220-230.

Nakano, T., and Harashima, S. (2024). Magnetic properties of Ca-containing zeolite low-silica X loaded with K atoms. *Interactions, 245*(1), 59.

Norby, P., Poshni, F. I., Gualtieri, A. F., Hanson, J. C., and Grey, C. P. (1998). Cation migration in zeolites: an in situ powder diffraction and MAS NMR study of the structure of zeolite Cs (Na)-Y during dehydration. *The Journal of Physical Chemistry B, 102*(5), 839-856.

Panda, D., Kumar, E. A., and Singh, S. K. (2019). Amine modification of binder-containing zeolite 4A bodies for post-combustion CO_2 capture. *Industrial & Engineering Chemistry Research, 58*(13), 5301-5313.

Ríos, J.-L. (2016). Essential oils: What they are and how the terms are used and defined. In *Essential oils in food preservation, flavor and safety* (pp. 3-10). Elsevier.

Rouquerol, F. (1999). Adsorption by clays, pillared layer structures and zeolites. *Adsorption by powders and porous solids*.

Salehi, S., and Anbia, M. (2017). Characterization of CPs/Ca-exchanged FAU-and LTA-type zeolite nanocomposites and their selectivity for CO_2 and N_2 adsorption. *Journal of Physics and Chemistry of Solids, 110*, 116-128.

Sharma, P., Jeong, S.-J., Han, M.-H., and Cho, C.-H. (2015). Influence of silica precursors on octahedron shaped nano NaY zeolite crystal synthesis. *Journal of the Taiwan Institute of Chemical Engineers, 50*, 259-265.

Siriwardane, R. V., Shen, M.-S., Fisher, E. P., and Losch, J. (2005). Adsorption of CO_2 on zeolites at moderate temperatures. *Energy & Fuels, 19*(3), 1153-1159.

Siriwardane, R. V., Shen, M.-S., Fisher, E. P., and Poston, J. A. (2001). Adsorption of CO_2 on molecular sieves and activated carbon. *Energy & Fuels, 15*(2), 279-284.

Strzemiecka, B., Kasperkowiak, M., Łoży**ń**ski, M., Paukszta, D., and Voelkel, A. (2012). Examination of zeolites as fragrance carriers. *Microporous and Mesoporous Materials, 161*, 106-114.

Tavasoli, M., Kazemian, H., Sadjadi, S., and Tamizifar, M. (2014). Synthesis and characterization of zeolite NaY using kaolin with different synthesis methods. *Clays and Clay Minerals, 62*(6), 508-518.

Tekin, R., and Bac, N. (2016). Antimicrobial behavior of ion-exchanged zeolite X containing fragrance. *Microporous and Mesoporous Materials, 234*, 55-60.

Tekin, R., Bac, N., Warzywoda, J., and Sacco Jr, A. (2015). Encapsulation of a fragrance molecule in zeolite X. *Microporous and Mesoporous Materials, 215*, 51-57.

Thommes, M., Kaneko, K., Neimark, A. V., Olivier, J. P., Rodriguez-Reinoso, F., Rouquerol, J., and Sing, K. S. (2015). Physisorption of gases, with special reference to the evaluation of surface area and pore size distribution (IUPAC Technical Report). *Pure and applied chemistry, 87*(9-10), 1051-1069.

Tsitsishvili, V. (2019). Transformation of natural analcime and phillipsite during their hydrothermal recrystallization into zeolites a and X. *Int. J. Adv. Res., 7*, 219-230.

Vaughn, J., Wu, H., Efremovska, B., Olson, D. H., Mattai, J., Ortiz, C., Puchalski, A., Li, J., and Pan, L. (2013). Encapsulated recyclable porous materials: an effective moisture-triggered fragrance release system. *Chemical Communications, 49*(51), 5724-5726.

Walton, K. S., Abney, M. B., and LeVan, M. D. (2006). CO_2 adsorption in Y and X zeolites modified by alkali metal cation exchange. *Microporous and Mesoporous Materials, 91*(1-3), 78-84.

Wang, Y., Du, T., Song, Y., Che, S., Fang, X., and Zhou, L. (2017). Amine-functionalized mesoporous ZSM-5 zeolite adsorbents for carbon dioxide capture. *Solid State Sciences, 73*, 27-35.

Wittayakun, J., Khemthong, P., and Prayoonpokarach, S. (2008). Synthesis and characterization of zeolite NaY from rice husk silica. *Korean Journal of Chemical Engineering, 25*, 861-864.

Yates, D. (1968). Studies on the surface area of zeolites, as determined by physical adsorption and X-ray crystallography. *Canadian Journal of Chemistry, 46*(10), 1695-1701.

Yilmaz, B., and Müller, U. (2009). Catalytic applications of zeolites in chemical industry. *Topics in Catalysis, 52*, 888-895.

Zhang, B., Huang, J., Liu, K., Zhou, Z., Jiang, L., Shen, Y., and Zhao, D. (2019). Biocompatible cyclodextrin-based metal-organic frameworks for long-term sustained release of fragrances. *Industrial & Engineering Chemistry Research, 58*(43), 19767-19777.

Zhang, C., Li, S., and Bao, S. (2019). Sustainable synthesis of ZSM-5 zeolite from rice husk ash without addition of solvents. *Waste and Biomass Valorization, 10*, 2825-2835.

Zouaoui, E. H., Djamel, N., Wan Ab Karim Ghani, W. A., and Samira, A. (2021). High-pressure CO_2 adsorption onto NAX zeolite: Effect of Li^+, K^+, Mg^{2+}, and Zn^{2+} and equilibrium isotherms study. *Iranian Journal of Chemistry and Chemical Engineering, 40*(4), 1195-1215.

Zukal, A., Arean, C., Delgado, M., Nachtigall, P., Pulido, A., Mayerová, J., and Čîejka, J. (2011). Combined volumetric, infrared spectroscopic and theoretical investigation of CO_2 adsorption on Na-A zeolite. *Microporous and Mesoporous Materials, 146*(1-3), 97-105.

APPENDIX

APPENDIX

Adsorption of wintergreen and eucalyptus essential oil on zeolites

Introduction

Essential oils (EO) are obtained from aromatic plants as secondary metabolites and characterized by their intense aroma. They have a wide range of applications due to their aromatic properties, such as perfumes, aromatherapy, health care, personal care products, and food preservation (Bakkali et al., 2008). However, essential oils are known to exhibit high volatility, leading to a reduced perception of their odor over time. Therefore, it is important to maintain the odor characteristics of essential oils for longer by encapsulating EO in porous materials.

Zeolites are crystalline aluminosilicates interconnected by corner-sharing $[SiO_4]_4^-$ and $[AlO_4]_5^-$. The framework contains different pore sizes, shapes and hydrophobic or hydrophilic properties. These unique characteristics of zeolites have led to various applications as catalysts, ion exchangers, and adsorbents (Tekin and Bac, 2016). Moreover, they have low toxicity, low cost and stable structure. Zeolite can be used as host materials for EO encapsulation and controlled release.

Researchers have tried to encapsulate fragrance molecules in porous materials such as cyclodextrin and metal-organic frameworks (MOFs). However, the major limitations of cyclodextrin and MOFs are high cost and toxicity. Then, an alternative way to encapsulate fragrances in porous material for controlled release of fragrance, such as zeolite. Costa et al. (2022) studied the encapsulation of different fragrances using two zeolite structures (FAU and MOR). The retention of fragrances in zeolite increased in the order NaX<NaY and NaMOR for cinnamaldehyde, limonene, methyl anthranilate, and vanillin. Tekin et al. (2015) encapsulated triplal using zeolite X with different average particle diameters (20 μm and 4 μm). The larger particles show a

slower release of triplal. Therefore, the properties of pore structure, crystal size, and chemical composition of zeolites have an influence on the adsorption and release behavior of fragrances. The interest in this work is encapsulated essential oils in different zeolite structures (NaA and NaX), Si/Al ratios (NaX and NaY), and crystal sizes for prolonged fragrance release.

Research objectives

1. To synthesize essential oils encapsulated in zeolites with difference structures, Si/Al ratios for long time release of essential oils.
2. To understand the adsorption and release behavior of fragrance from zeolites.

Literature review

Essential oils

Essential oil (EO) is a volatile fragrant that is extracted from plant material through the process of steam distillation. Several EOs exhibit highly promising biological applications, as they are non-toxic at very low concentrations (Ríos, 2016). They are commonly used in various products, including perfumes, personal care items, food preservation, and healthcare.

Methyl salicylate is the major constituent found in wintergreen oil, which is obtained through the distillation of wintergreen leaves. It possesses analgesic properties and is commonly utilized in analgesic creams or gels intended for topical application. The effects of methyl salicylate are multifaceted, exhibiting analgesic, anti-inflammatory, and counterirritant properties (Dasgupta et al., 2014).

The oil of eucalyptus is extracted through distillation from the fresh leaves of different Eucalyptus species. It is a colorless or pale-yellow liquid with a distinct aroma and camphoraceous odor. When tasted, it has a pungent, camphor-like flavor that is followed by a cooling sensation. Eucalyptus oil is widely used for relieving symptoms associated with nasopharyngeal infections. It can be consumed internally in the form of mixtures or inhaled for its therapeutic benefits (Evans and Evans, 2009).

As essential oil compounds are highly volatile, encapsulating them within porous materials provides the capability to control the release of the molecules and protect them from evaporation.

Encapsulation of fragrances in porous material

Porous materials are a class of substances characterized by the presence of voids or pores within their structure. Examples of such materials include cyclodextrin, metal-organic frameworks (MOFs), silica nanoparticles, activated carbon, and zeolites. These materials have found widespread application as support or carriers for the controlled release of various fragrances. They exhibit good storage, high porosity, and greater adsorbability, which depends upon the properties of pore structure, molecular structure, and the interaction of fragrance molecules with porous materials.

Metal–organic frameworks (MOFs) are porous materials that have become a prominent category of crystalline materials characterized by their exceptional porosity, reaching up to 90% free volume, and vast internal surface areas that exceed 6,000 m^2/g. These properties, MOFs have found a wide range applications in industrial fields such as gas adsorption, heterogeneous catalysis, and controlled release of fragrances.

Cyclodextrins are macrocyclic compounds with a truncated cone-like structure formed by linking oligosaccharides through α-1,4-glucosidic bonds. These cyclodextrins, often abbreviated as CDs, are extensively utilized in host-guest chemistry for encapsulating target molecules within their cavities. The use of cyclodextrin complexes as controlled release systems has enabled their application in various biocompatible domains, encompassing functional foods and drug delivery. Moreover, this capability has paved the way for their use in encapsulating and releasing flavors and fragrances, preserving the product's original organoleptic properties for consumers.

B. Zhang et al. (2019) reported the encapsulation of fragrances in γ-cyclodextrin (γ-CD)-based MOFs for controlled release of fragrances. In comparison to γ-CD and γ-CD-MOFs, the γ-CD-MOF showed higher encapsulation capability and

prolonged fragrance release due to the enhanced host–guest hydrophobic and hydrogen bonding interactions of their porous structures.

However, the major limitations of MOFs and cyclodextrin are toxicity and high cost. Therefore, an alternative way to encapsulate fragrances in porous material for control of the release rate of scents is zeolite. Zeolite is a candidate for prolonged fragrance release because it is non-toxic, low-cost, and considered green.

Encapsulation of fragrances in zeolites

Zeolites are crystalline aluminosilicates containing pores and cavities. The primary structural units of zeolites are the tetrahedra of silicon and aluminum. They are applied for catalysis, ion exchange, and adsorption. The differences in the structure, morphology, hydrophobic/hydrophilic properties, pore size, crystal size, and chemical composition of zeolites have an influence on the adsorption ability of essential oils. Zeolites LTA and FAU structures, including NaA, NaX, and NaY, are interesting in this work. NaX and NaY zeolites have the same FAU structure but differ in their Si/Al ratios. Specifically, NaX has a Si/Al ratio of 1-1.5, while NaY has a Si/Al ratio greater than 1.5.

Table A1 shows examples of encapsulation of fragrances in porous materials. Eucalyptus essential oil can be encapsulated in zeolites Y covalently with β-cyclodextrins. The results in the table showed that the synthesized zeolites exhibited superior efficiency in encapsulating eucalyptus essential oil compared to free β-cyclodextrins. Additionally, they were effective in reducing the release kinetics of the oil.

Table A1 Example of encapsulation of fragrances in porous materials.

Materials	Fragrance (FG)	Result	Ref.
Natural zeolite (Micro 20) and synthesis molecular sieve (MSU-S)	Citral, p-cymene, geraniol, menthol	MSU-S is a better adsorbent of FG than micro-20.	Strzemieck a et al. (2012)

Table A1 (Continued) Example of encapsulation of fragrances in porous materials.

Materials	Fragrance (FG)	Result	Ref.
NaX	Triplal	Larger particles have lower desorption rates.	Tekin et al. (2015)
Recyclable porous material (RPMs)	Ethyl butyrate (EB) and D-limonene (DL)	FG release rates: EB@RPM (1 h) > DL@RPM (1.5 h)	Vaughn et al. (2013)
NaY NaX NaY NaMOR	D-limonene Cinnamaldehyde Methyl anthranilate Vanillin	Fast release in 2 weeks Fast release in 2 weeks Release at longer time (720 days) Release at longer time (720 days)	Costa et al. (2022)
NaYCDsuc NaYCDadi NaYCDcit	Eucalyptus essential oil (EEO)	Modified zeolites reduced the release of EEO more efficiently than free EEO	Mallard et al. (2018)
Rice husk	Methyl salicylate (MS)	Rice husk (RH) bio sorbents from agricultural waste had the potential to release MS slowly for delayed ripening in Namwa bananas.	Cholmaitri et al. (2020)

In this work, essential oils will be encapsulated in zeolites with different structures, including NaA, NaX, and NaY zeolites. The synthesized zeolites and

encapsulated essential oils in zeolites was characterized by X-ray diffraction (XRD), scanning electron microscopy (SEM), thermogravimetric analysis (TGA), Fourier transform infrared spectrometry (FTIR), and N_2 adsorption analysis.

Research procedure

Chemicals and materials

Chemicals for synthesis NaA, NaX, and micron NaY zeolites are fumed silica (99.8% SiO_2, Sigma-Aldrich), sodium aluminate (41.383% Na_2O, 58.604% Al_2O_3, Riedel-de Haën®), and sodium hydroxide (97%wt NaOH, Carlo-Erba). The chemical for the preparation of solution B of nano NaY is Ludox® HS-40 colloidal silica (40%wt silica suspension in H_2O).

Synthesis of zeolite NaA by using fumed silica as a silica source

Synthesis of zeolite NaA, NaX, NaY

Zeolite NaA was synthesized with the same gel ratio and procedure as in Section 3.12, 3.13, and 3.14. Fumed silica was used as a silica source.

Material characterization

The synthesized zeolites were characterized by XRD, FTIR, SEM-EDS, and N_2 adsorption-desorption analysis as reported in Section 3.2.

Results and Discussion

Characterization of zeolite NaA

Figure A1 shows the XRD patterns of the synthesized zeolite. The characteristic XRD peaks of zeolite NaA appear at $2\theta \sim 7°$, 10 and ~ 12°. These peaks are narrow and sharp, indicating the high crystallinity and purity of the product.

FTIR spectra of zeolite NaA (Figure A2) shows characteristic zeolite bands related to zeolite structures. The band at 460 cm^{-1} indicating Si-O bending vibration of Si-O-Si, at 550 cm^{-1} indicating Si-O stretching vibration of Si-O-Si, at 660 cm^{-1} indicating Si-O stretching vibration of O-Si-O, at 1000 cm^{-1} indicating O-Al-O asymmetry stretch

vibration, at 1600 cm^{-1} indicating Si-OH bending vibration, and at 3400 cm^{-1} indicating -OH stretch vibration of Si-OH.

Figure A3 presents the SEM images of synthesized zeolite NaA, showing cubic morphology of 0.2-1 μm. Its Si/Al ratio was 1.04.

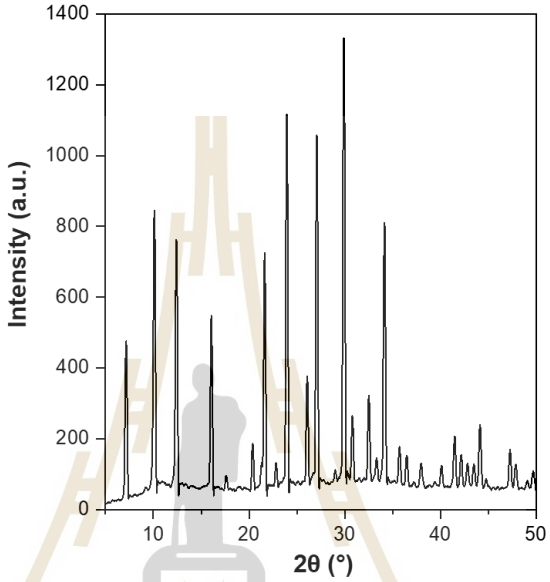

Figure A1 The XRD pattern of zeolite NaA.

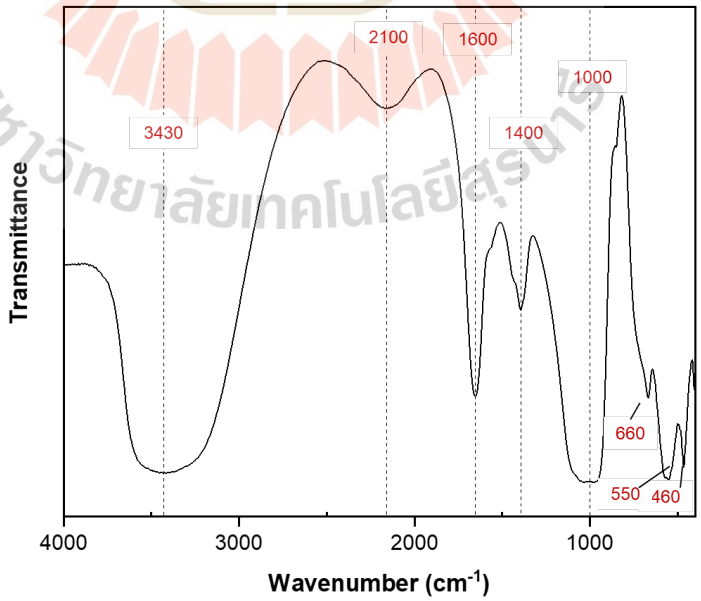

Figure A2 FTIR spectra of zeolite NaA.

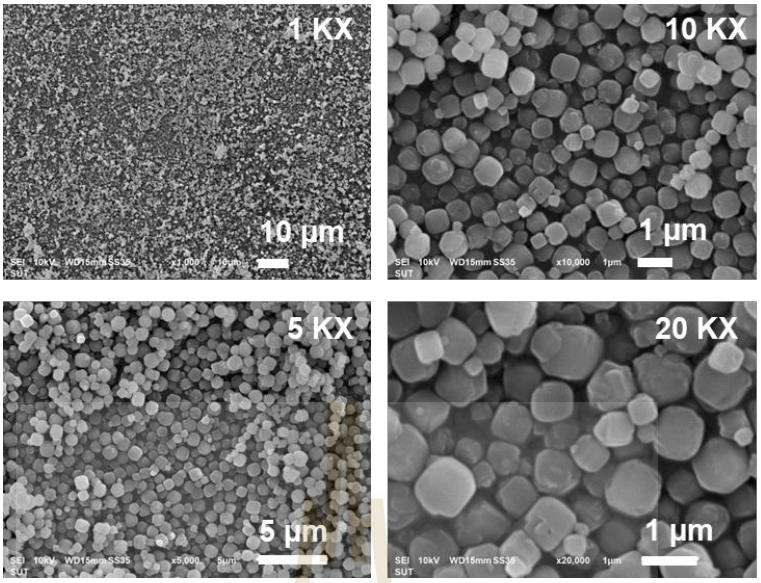

Figure A3 SEM images of zeolite NaA with a magnification of 1, 5, 10 and 20 KX.

Characterization of zeolite NaX

Figure A4 shows the XRD patterns of the synthesized zeolite NaX showing the FAU characteristic peaks. Its FTIR spectra (Figure A5) shows the band of Si-O-Si bending at 444 cm^{-1}, Si-O-Si stretching at 675 cm^{-1}, O-Si-O stretching at 746 cm^{-1}, O-Al-O asymmetric stretching at 1000 cm^{-1}, Si-OH bending at 1648 cm^{-1}, Si-OH stretch at 3433 cm^{-1}. The SEM image (Figure A6) confirmed the non-uniform polycrystal morphology of zeolite NaX with Si/Al ratio 1.33.

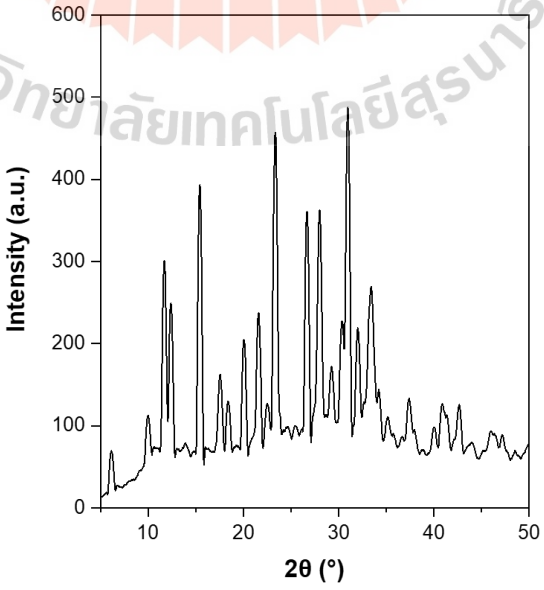

Figure A4 The XRD pattern of zeolite NaX by using fumed silica as silica source.

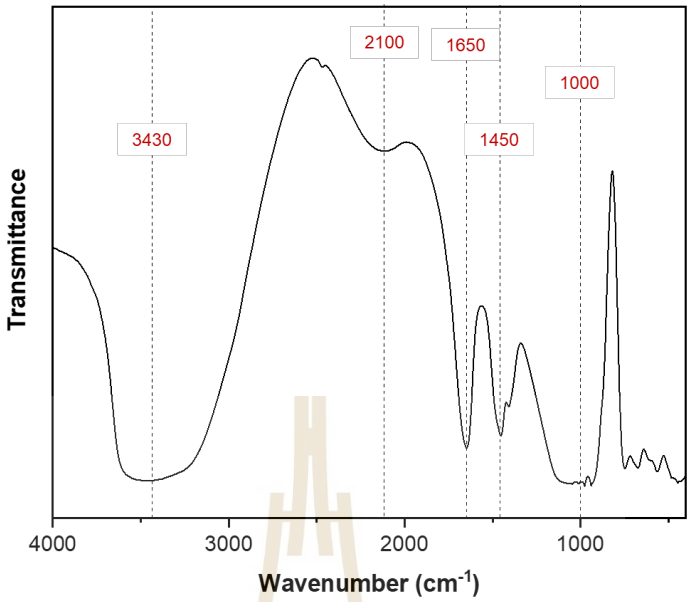

Figure A5 FTIR spectra of zeolite NaX by using fumed silica as silica source.

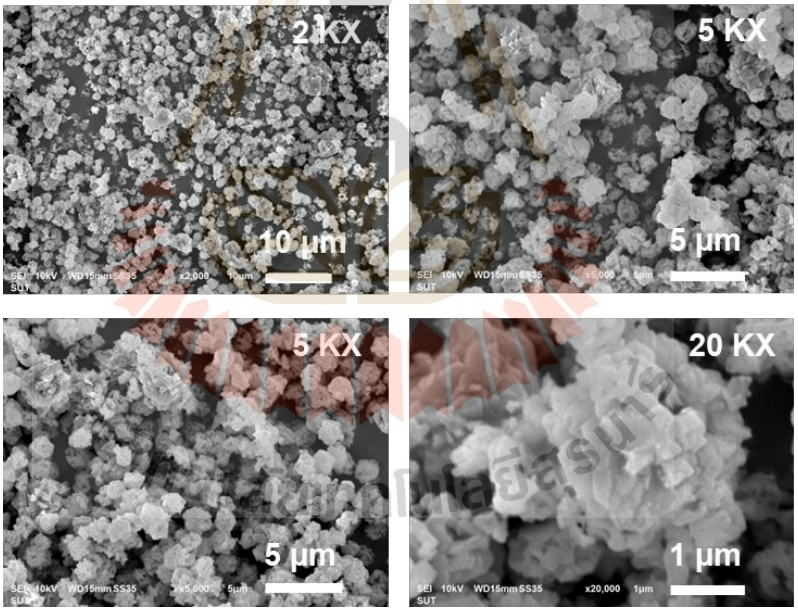

Figure A6 SEM images of zeolite NaX by using fumed silica as silica source with a magnification of 2, 5 and 20 KX.

Characterization of zeolite NaY

Figure A7 shows the XRD pattern of pure-phase zeolite NaY with sharp peaks, consistent with most of the reports on the diffraction peaks at 2θ ~ 6°, 10 and ~ 15°. Figure A8 shows its FTIR spectra with bands at 450 cm^{-1} (Si-O-Si bending), at 572 cm^{-1}

(Si-O-Si stretching), at 699 cm^{-1} (O-Si-O stretching), at 1030 cm^{-1} (O-Al-O asymmetric stretching), at 1644 cm^{-1} (O-Si-OH bending), at 3466 cm^{-1} (Si-OH stretching). This sample presents an agglomerate of polyhedral morphology with Si/Al ratio 2.19 (Figure A9).

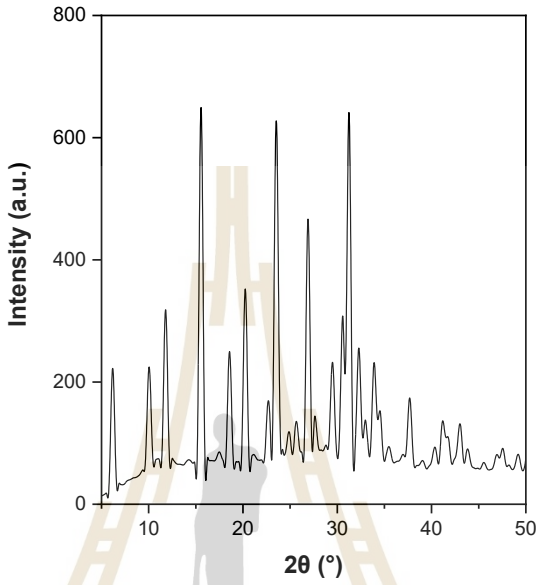

Figure A7 The XRD pattern of zeolite NaY by using fumed silica as silica source.

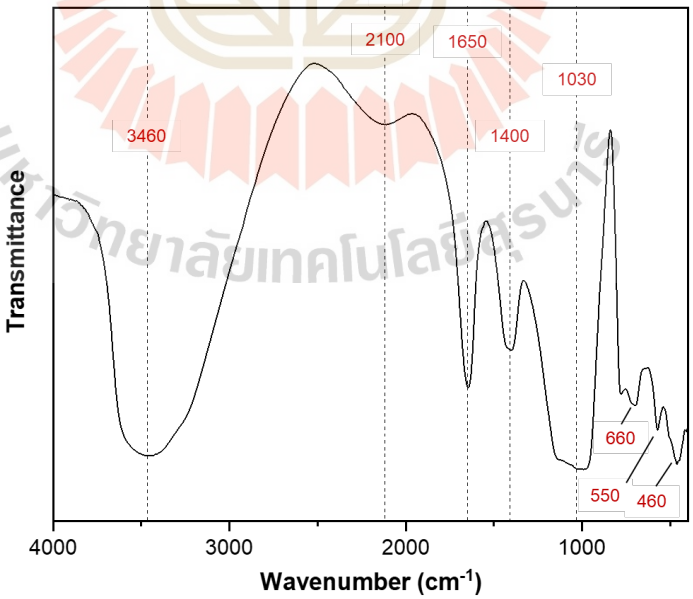

Figure A8 FTIR spectra of zeolite NaY by using fumed silica as silica source.

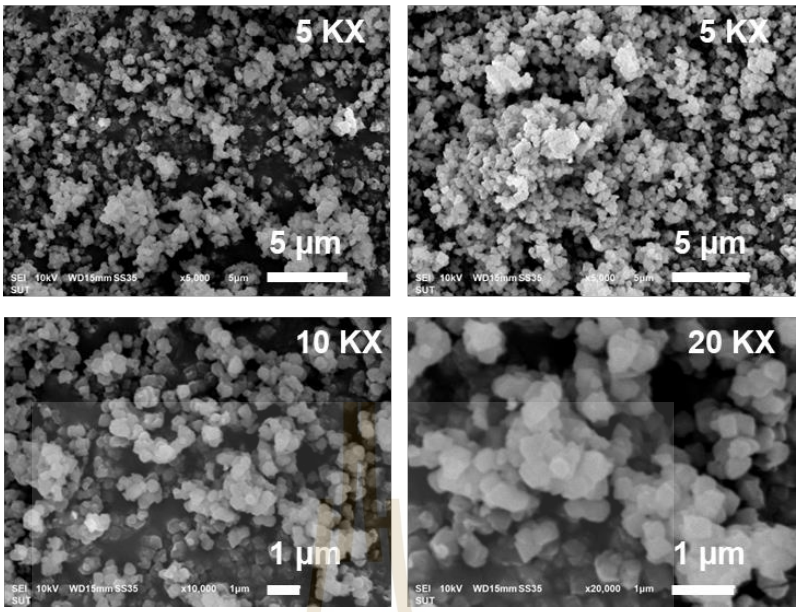

Figure A9 SEM images of zeolite NaY by using fumed silica as silica source with a magnification of 5, 10 and 20 KX.

Preparation of encapsulated essential oils (EO) in zeolites

The encapsulation of essential oils was conducted with the procedure from Costa et al. (2022). Samples were prepared by dissolving 0.4 mmol essential oils in 10 mL of ethanol and adding to 1.5 g of NaA, NaX, micron NaY zeolites, respectively. Fragrance encapsulation was performed by adding solutions with zeolites in a 125 mL PP bottle and allowing it to stir (300 rpm) for 72 h at room temperature (25±5 ˚C). After that, the samples was centrifuged at 4000 rpm for 3 min and dried EO/zeolites at 40 ˚C for 72 h to remove the ethanol. Then, the supernatant solutions and EO/zeolites was stored in glass flasks sealed with parafilm and placed in a refrigerator to prevent evaporation and maintain a closed system.

Release fragrance from zeolites

The encapsulated methyl salicylate (MS) in zeolites was stored in vials sealed with parafilm, and these were placed in desiccators at room temperature (24±5 ˚C). The methyl salicylate release experiments were carried out at room temperature during 0-5 h. The amount of essential oils from zeolites and the release profiles was monitored using the thermogravimetric (TGA) analysis. The TGA was performed by

Mettler Toledo model TGA/DSC1 in N_2 gas with a flow rate of 50 mL/min at a heating rate of 10 °C/min up to 350 °C.

The TGA profiles of all the adsorption methyl salicylate in synthesized zeolites samples (Figure A10-A13) show two regions of weight loss. The first is attributed to the desorption of water in the zeolite structure (80-250 °C). The second attributed to the decomposition of methyl salicylate at 100-220 °C. Therefore, this result cannot determine the amount of methyl salicylate in zeolites because the peak of water overlaps with a peak of methyl salicylate.

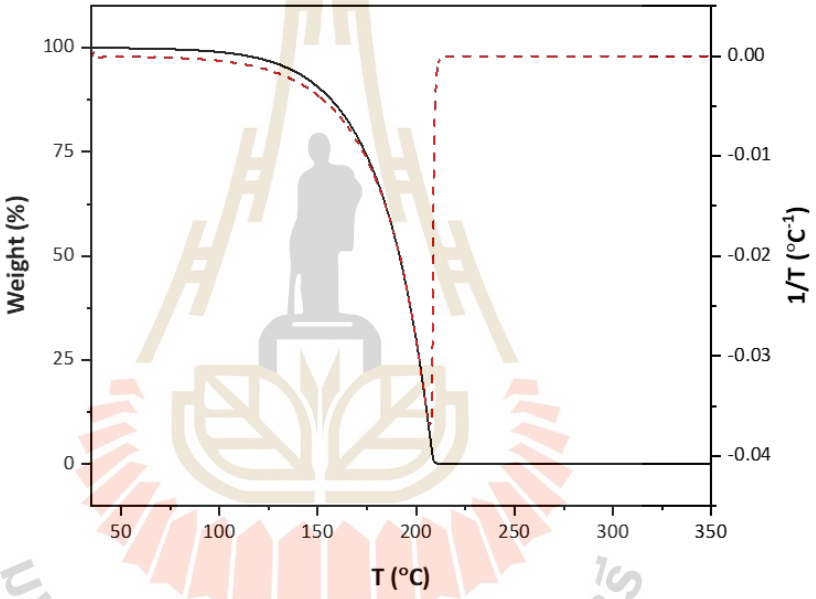

Figure A10 TGA curve of liquid methyl salicylate.

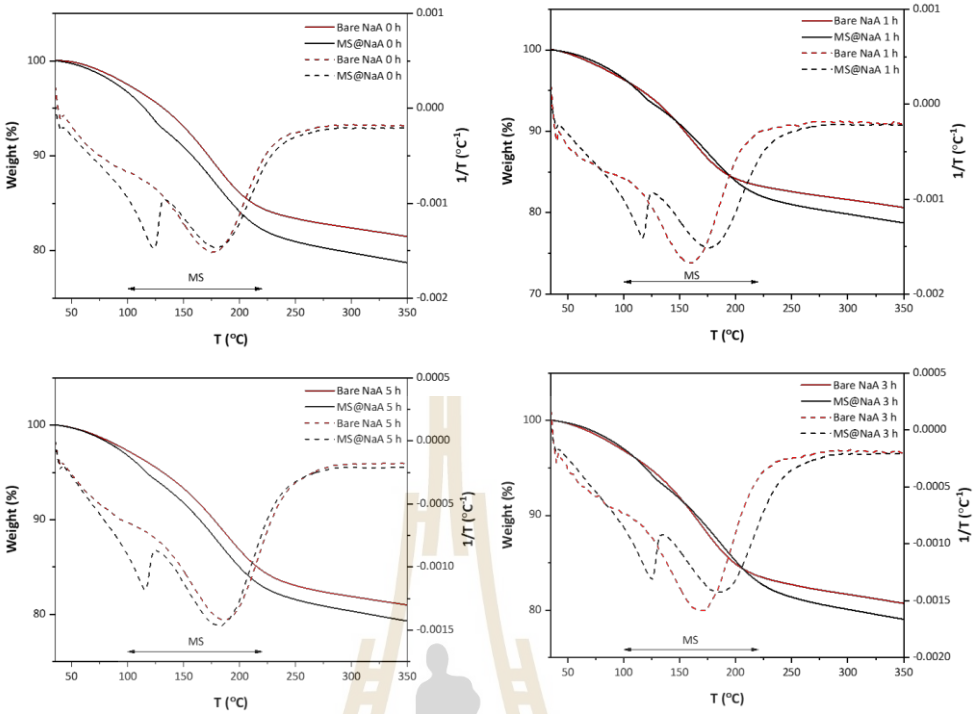

Figure A11 TGA curve of MS@NaA and bare NaA (time = 0, 1, 3 and 5 h).

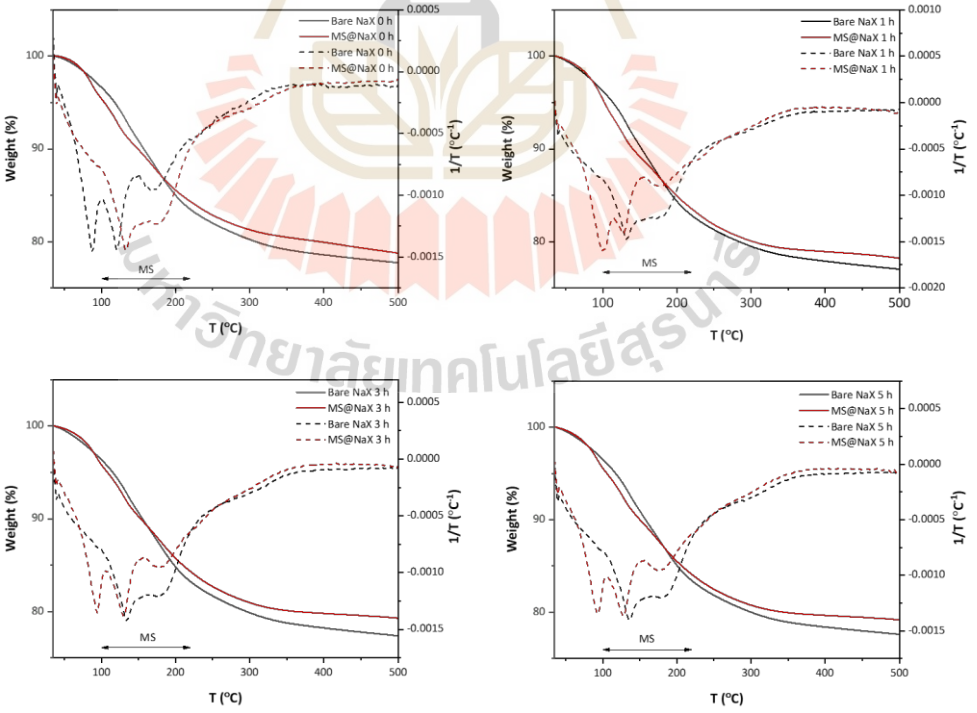

Figure A12 TGA curve of MS@NaX and bare NaX (time = 0, 1, 3 and 5 h).

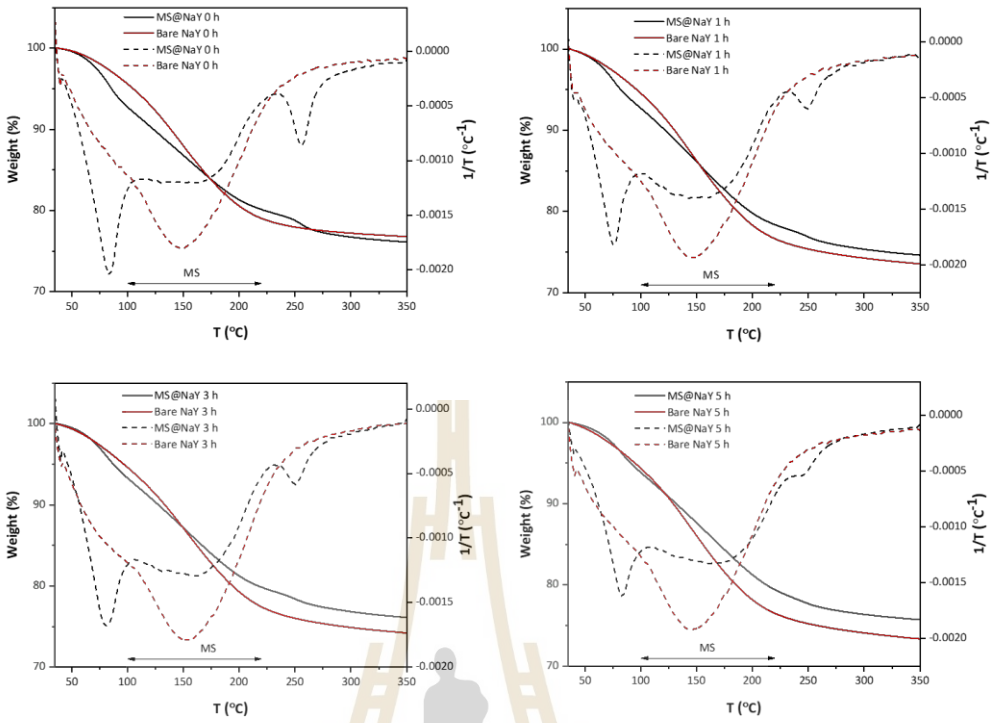

Figure A13 TGA curve of MS@NaY and bare NaY (time = 0, 1, 3 and 5 h).

Adsorption of methyl salicylate in zeolites by solid-gas adsorption

At the beginning of the temperature-programmed experiment (pre-heat zeolite), 0.1 g of zeolite powder was put into the tube, and then the tube was heated by tube furnace at 200 °C for 2 h with N_2 gas was introduced into the tube. After the temperature of the furnace had cooled down to room temperature, the power of the furnace was shut off while the N_2 was continued in the experiment.

The liquid of methyl salicylate was heated at 120 °C in an oil bath, and N_2 gas was passed through a gas bubbler containing essential oils to introduce essential oils vapor into the zeolites at room temperature for 1, 3, and 6 h. Figure A14 shows a Diagram of the adsorption of methyl salicylate in zeolites by solid-gas adsorption.

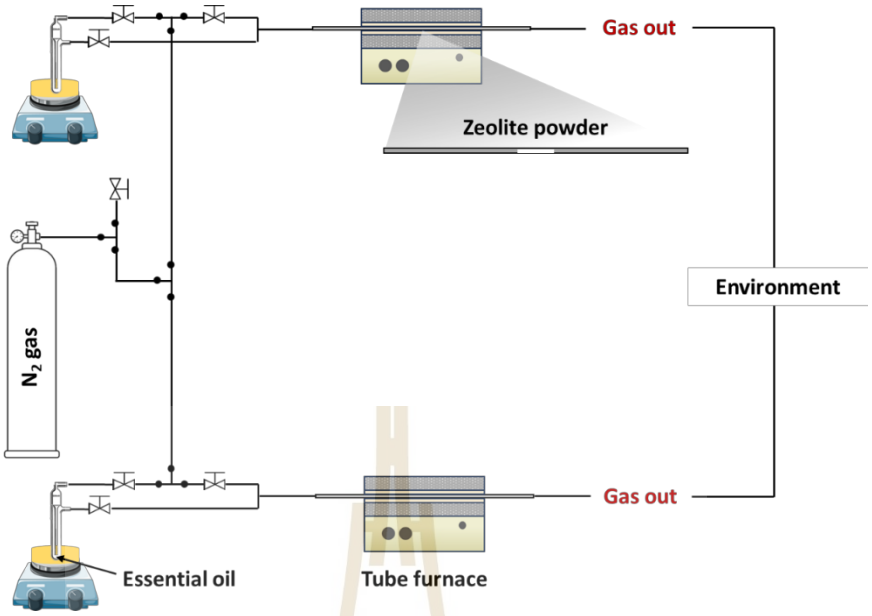

Figure A14 Diagram of adsorption essential oils in zeolites by solid-gas adsorption.

Determine the amount of methyl salicylate in zeolites by GC-FID

The amount of methyl salicylate in zeolite was analyzed by Gas chromatography-flame ionization detection (GC-FID). Heated zones were set at 220 °C for injection and detector port. The initial oven temperature was 80°C and was maintained for 4 min. It was then heated at 10°C/min to 220 °C and held for 3 min. All samples were injected manually at a volume of 1 µL.

Preparation of standard solutions

Standard solutions of methyl salicylate 5 mL were prepared by dissolving it in ethanol at concentrations 250, 500, 1000, 1500, 2000, 3000, and 4000 ppm. Nitrobenzene 40 µL used as the internal standard for methyl salicylate. Figure A15 shows the calibration curve of standard solutions.

Preparation of sample solutions

Sample solutions were prepared by dissolving 2 mL of ethanol in a 20 mL vial and stirring at 100 ± 5 °C for 24 hours to extract methyl salicylate from the zeolite for GC analysis. The samples were then filtered using a 0.22 µm syringe filter.

Next, 1000 µL of the filtrate and 40 µL of nitrobenzene were transferred into a 10 mL volumetric flask. The flask was then filled with ethanol up to the calibration mark to prepare the solution for methyl salicylate determination in zeolites.

Figures A16-A24 show the adsorption of methyl salicylate in synthesized zeolites in different adsorption times. The retention times of ethanol (solvent) and nitrobenzene (internal standard) were 0.2 and 3 min, respectively. The peak of methyl salicylate was not observed in all samples. These results show that methyl salicylate cannot access zeolites.

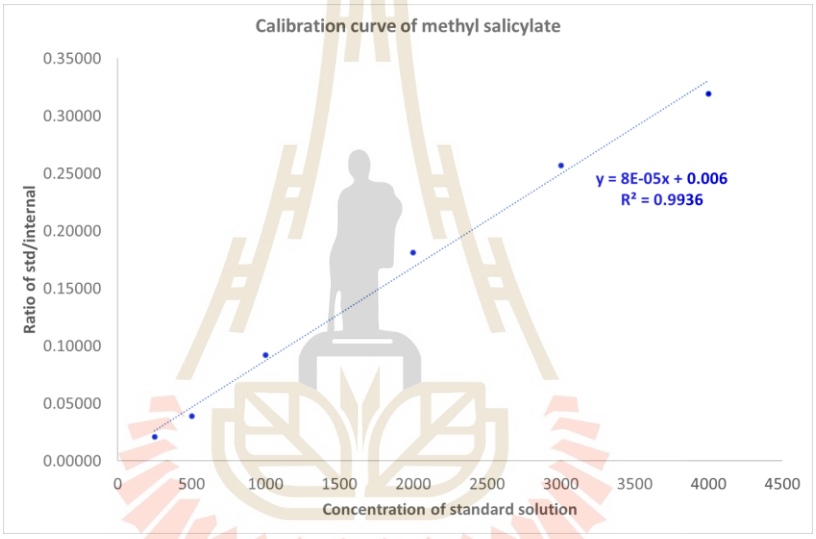

Figure A15 Calibration curve of standard solutions.

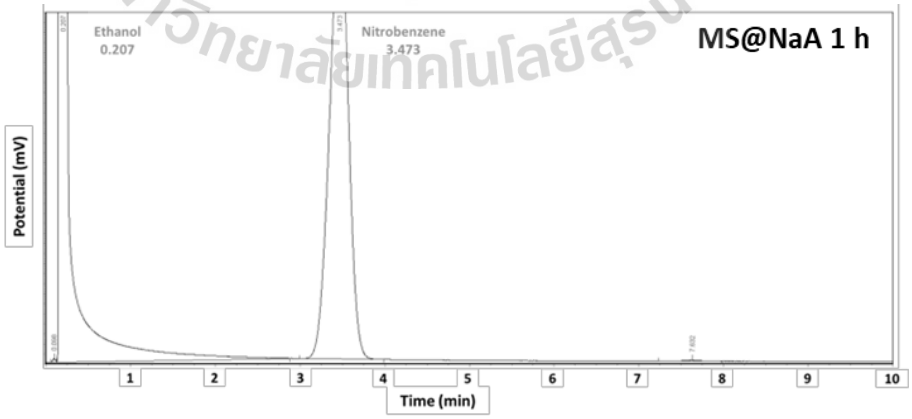

Figure A16 Gas chromatogram of methyl salicylate adsorbs on zeolite NaA for 1 h.

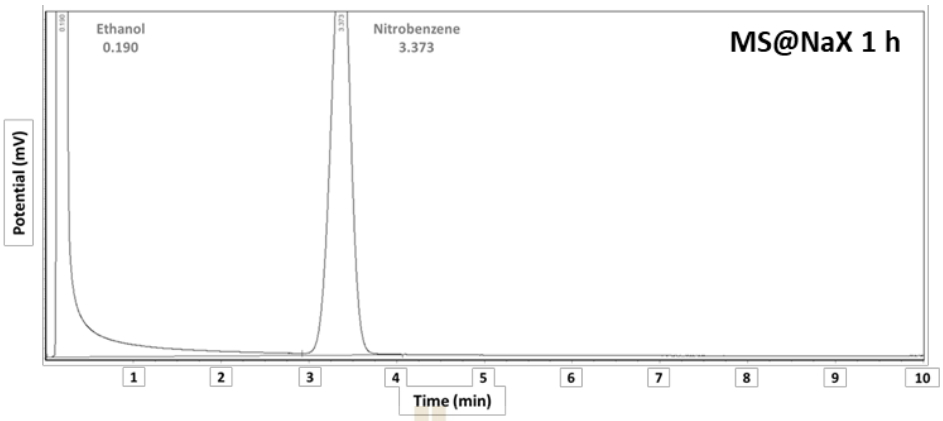

Figure A17 Gas chromatogram of methyl salicylate adsorbs on zeolite NaX for 1 h.

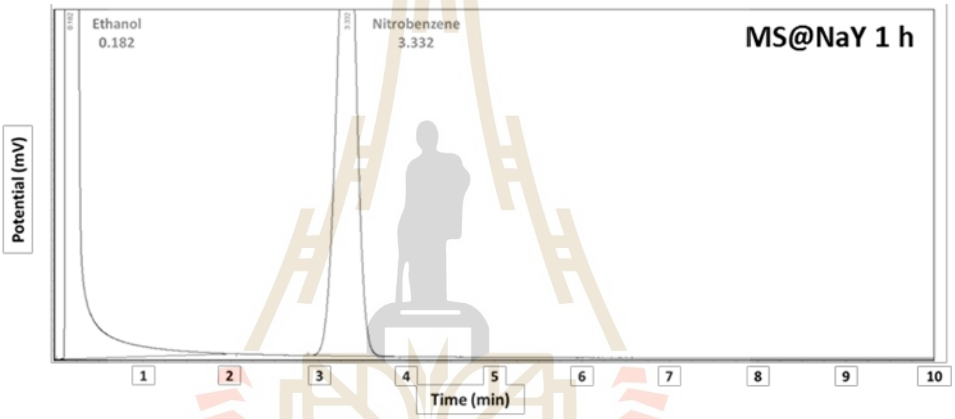

Figure A18 Gas chromatogram of methyl salicylate adsorbs on micron-sized zeolite NaY for 1 h.

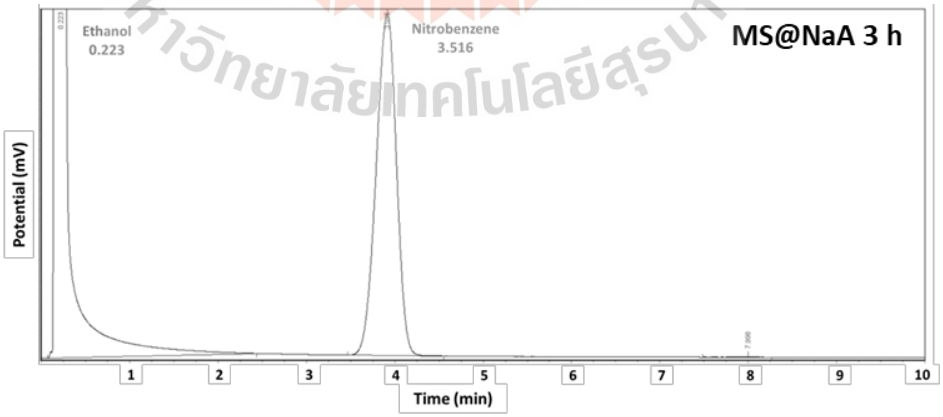

Figure A19 Gas chromatogram of methyl salicylate adsorbs on zeolite NaA for 3 h.

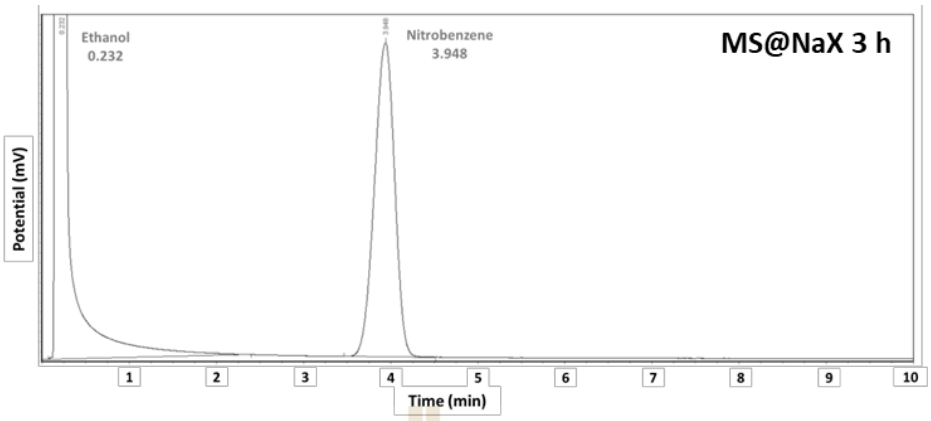

Figure A20 Gas chromatogram of methyl salicylate adsorbs on zeolite NaX for 3 h.

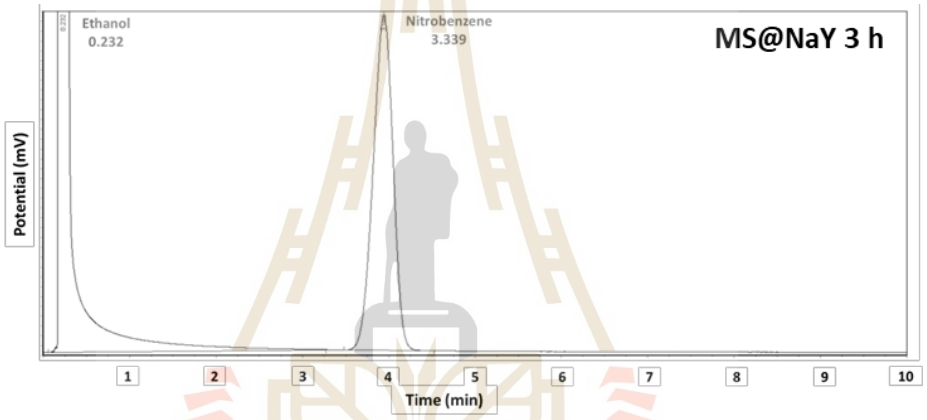

Figure A21 Gas chromatogram of methyl salicylate adsorbs on micron-sized zeolite NaY for 3 h.

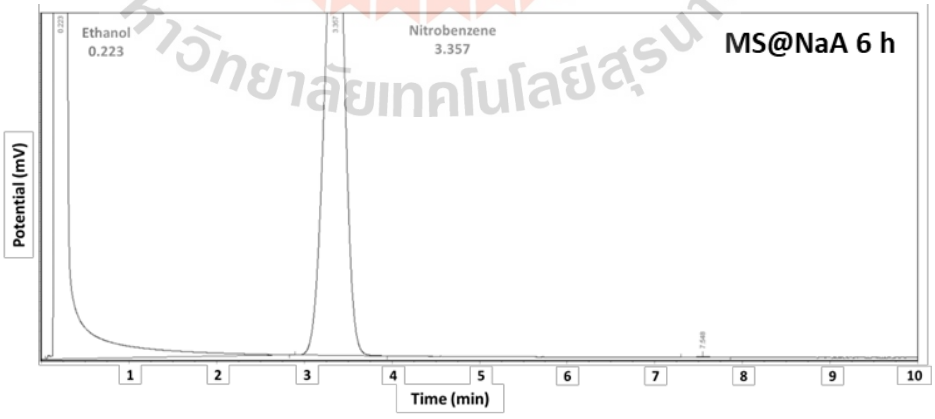

Figure A22 Gas chromatogram of methyl salicylate adsorbs on zeolite NaA for 6 h.

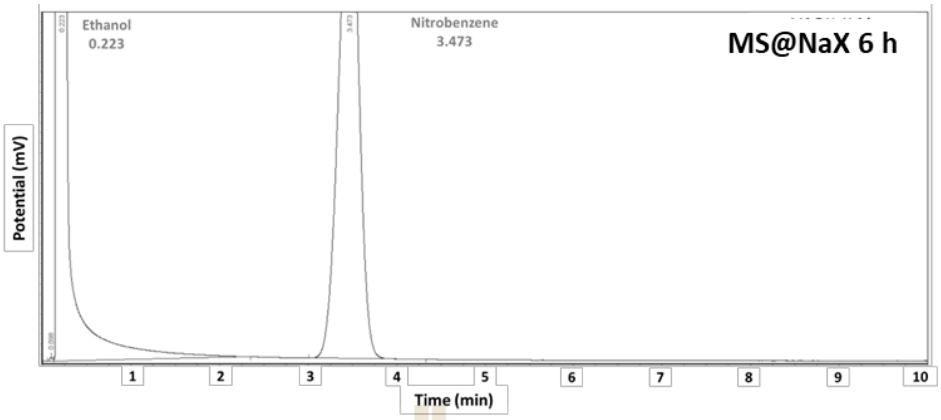

Figure A23 Gas chromatogram of methyl salicylate adsorbs on zeolite NaX for 6 h.

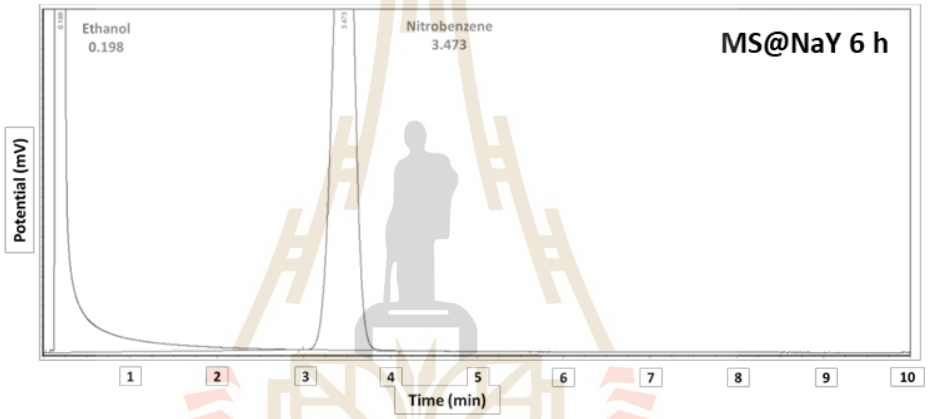

Figure A24 Gas chromatogram of methyl salicylate adsorbs on micron-sized zeolite NaY for 6 h.

CURRICULUM VITAE

NAME	Miss Chalida Upan
Date of Birth	November 2nd, 1999
Place of Birth	Mukdahan, Thailand

Education

2018 - 2022	B.Sc. (Chemistry), Suranaree University of Technology (SUT), Nakhon Ratchasima, Thailand
2022 - present	M.Sc. (Chemistry), Suranaree University of Technology (SUT), Nakhon Ratchasima, Thailand

Grants and Fellowships

2018 – 2022	Quota scholarship for students with special talents in science and technology
2022 – 2024	Scholarship for undergraduate students with academic achievement